Asian emissions of CO and NO$_x$:
Constraints from aircraft and Chinese station data

Yuxuan X. Wang and Michael B. McElroy

Department of Earth and Planetary Science and Division of Engineering and Applied Sciences, Harvard University,
Cambridge, Massachusetts, USA

Tao Wang

Department of Civil and Structural Engineering, Hong Kong Polytechnic University, Hong Kong, China

Paul I. Palmer

Department of Earth and Planetary Science and Division of Engineering and Applied Sciences, Harvard University,
Cambridge, Massachusetts, USA

[1]   Observations of CO and NO$_y$ from the Transport and Chemical Evolution over the Pacific (TRACE-P) aircraft mission over the northwest Pacific and from two Chinese ground stations (Hong Kong and Lin An) during spring 2001 are used in conjunction with an optimal estimation inverse model to constrain estimates of Asian emissions of CO and NO$_x$. A priori emissions are based on a detailed bottom-up inventory for the observation period. The inversion analysis requires 43% and 47% increases in Chinese emissions of CO and NO$_x$, respectively, distributed heterogeneously, with the largest adjustments required for central China. A posteriori estimates of emissions from biomass burning in Southeast Asia are much lower than a priori values. Inversion results for NO$_x$ emissions are consistent with CO emissions in terms of the sense of the adjustments. Inclusion of the station data in the inversion analysis significantly improves estimates for emissions from central and south China. A large increase in NO$_x$ emissions inferred for central China (a factor of 3) is attributed to decomposition of organic wastes associated with the human-animal food chain and extensive applications of chemical fertilizer. An analysis of emission ratios for CO relative to NO$_x$ for different sectors indicates that emissions attributed to industry and transportation may be underestimated in the bottom-up inventory for central China, while emissions from the domestic sector may be underestimated for south China. An increase in emission factors could help reconcile results from the inversion analysis with the "bottom-up" approach. Detailed analysis of the surface observations using a posteriori emissions indicates the importance of meteorological phenomena, notably cold fronts in March and small-scale high- and low-pressure systems in April in modulating concentrations of CO, with the latter most evident in the data from Lin An.   INDEX TERMS: 0365 Atmospheric Composition and Structure: Troposphere—composition and chemistry; 0345 Atmospheric Composition and Structure: Pollution—urban and regional (0305); 0368 Atmospheric Composition and Structure: Troposphere—constituent transport and chemistry; KEYWORDS: inversion, Asian emissions, carbon monoxide, nitrogen oxides

1.   Introduction

[2]   Rapid industrial development over the past 20 years in east Asia and specifically in China has resulted in unprecedented growth in emission of important gaseous and particulate components of the atmosphere with implications for both the global and regional environment. An important objective is to define the nature and extent of these emissions and to develop policies to mitigate their impact. Three-dimensional chemical transport models in combination with high-quality atmospheric measurements can play a critical role in addressing this challenge. Uncertainty in our understanding of relevant emissions poses a particular problem, however, in realizing the potential of this approach.

[3]   Emissions of a particular species may be estimated on the basis of a consideration of specific industrial and human activities, power generation fueled by combustion of coal for example, combined with data on related emissions. This

is usually referred to as a bottom-up approach. Activity rates may be obtained using publicly available data for individual sectors of a national economy (quantities of coal consumed in power generation, quantities of natural gas consumed in fertilizer manufacture, etc). Emission factors must be inferred from suitably targeted measurements for species of interest. The accuracy of emissions obtained using this approach depends obviously on the accuracy of the available economic data and on the accuracy and relevance of data available to define the associated emission factors. While data for developed economies such as Japan may be adopted with some confidence, data for developing economies such as China are more uncertain. Uncertainties in the latter case relate not only to the activity data [*Sinton and Fridley*, 2000] but also, even more consequentially, to the emission factors for which the available information is generally sparse, often based on only a few measurements or more commonly on application of data for specific technologies obtained elsewhere.

[4] The bottom-up approach was used by *Streets et al.* [2003] to develop an inventory of emissions for a variety of species for Asia in 2000. Their study was implemented in support of a series of intensive airborne measurement campaigns conducted over the NW Pacific in 2001: the Transport and Chemical Evolution over the Pacific (TRACE-P) mission and the Asian Pacific Regional Aerosol Characterization Experiments (ACE-Asia). Comparisons of model results for CO obtained using the emission inventory prepared by *Streets et al.* [2003] provide compelling evidence that emissions obtained in the bottom-up approach were too low, specifically for central and south China [*Carmichael et al.*, 2003; *Palmer et al.*, 2003; *Y. Wang et al.*, 2004]. *Palmer et al.* [2003] showed, for example, through a formal inverse model analysis, that a 54% increase in anthropogenic CO emissions in China would be required to reconcile model results with observation. *Carmichael et al.* [2003] suggested that emissions of CO from domestic coal burning in central China may have been underestimated in the bottom-up inventory while *Suntharalingam et al.* [2004] pointed to possible additional problems associated with underestimates of emissions from the power sector. Unresolved is whether other factors, such as biofuel combustion in household environments or fossil fuel combustion in other sectors of the Chinese economy, may also have contributed to the underestimate of CO emissions [*T. Wang et al.*, 2002]. It is clear that further work is required to refine current understanding of emissions of CO from China and as we shall see there are concerns also with bottom-up inventories for other species, notably for NO$_x$.

[5] This paper describes a reanalysis of the aircraft observations complemented by a study of data from two stations in China. The Chinese observations, reported by *T. Wang et al.* [2003, 2004], were taken at a remote coastal site (Hok Tsui) in Hong Kong (22°13′N, 114°15′E) and at a comparably remote rural site (Lin An) in east coastal China (30°25′N, 119°44′E). They provide a record of continuous, high-frequency variations in the concentrations of CO, O$_3$, NO, NO$_y$, and SO$_2$ for the spring of 2001, overlapping in time with the aircraft measurements. Although relatively remote, that is to say proximate sources of emission are comparatively small, these stations are not far removed

from the densely populated, industrialized, environments of the Pearl River Delta (PRD) and the Yangtze River Delta (YRD). Hourly mean concentrations of CO at Hok Tsui averaged 404 ppb, while the hourly average for Lin An was 677 ppb, which may be compared with average concentrations of 214 ppb and 121 ppb reported by *Parrish et al.* [1991] for two rural sites in the United States. An objective of the present study is to assess the improvements in emission estimates for China that can be realized as a consequence of integrating the ground-based measurements of near source environments with the TRACE-P aircraft measurements of continental outflow over the NW Pacific [*Jacob et al.*, 2003].

[6] The present study adopts the nested grid version of the GEOS-CHEM model described by *Y. Wang et al.* [2004]. This allows for a spatial resolution of 1° × 1° in a window region covering most of Asia embedded in a global background treated at a resolution of 4° × 5°. Use of the high-resolution window allows us to account for the important heterogeneity of emissions over the Asian region. In particular it allows us to account for important regional differences for China in terms of population, economic development, energy consumption, industrial activities and emission factors. Previous inverse studies either treated China as a whole [*Palmer et al.*, 2003] or aggregated east Asia as a single unit [*Kasibhatla et al.*, 2002; *Arellano et al.*, 2004]. In our earlier study using the high-resolution nested grid version of the CTM [*Y. Wang et al.*, 2004], we showed that emissions from different regions of China (south versus north, for example) follow different paths as they are exported to the Pacific. TRACE-P observations record therefore signatures of different source regions that can be resolved using the current model. The surface stations included in the present study are located in geographically distinct regions of China. Observations from these stations in combination with the aircraft data may be expected to provide useful additional constraints on the regional distribution of emissions from China.

[7] The present study focuses on emissions of carbon monoxide (CO) and nitrogen oxides (NO$_x$ = NO + NO$_2$). Reaction with OH represents the dominant sink for CO in the atmosphere contributing to a lifetime of several months under winter and spring conditions. The relatively long lifetime and simple chemistry of CO make it an ideal tracer for inverse studies that assume a linear relationship between sources and concentrations [*Kasibhatla et al.*, 2002; *Palmer et al.*, 2003; *Arellano et al.*, 2004]. Unlike CO, NO$_x$ undergoes complicated nonlinear chemical transformations in the troposphere on a timescale of minutes to hours. The sum of NO$_x$ and all of the compounds formed as products of its oxidation (including HNO$_3$, N$_2$O$_5$, NO$_3$, HNO$_4$, PAN, other organic nitrate, and aerosol nitrate) is conventionally defined as the family of reactive nitrogen, denoted as NO$_y$. As a family, NO$_y$ is lost from the atmosphere by dry and wet depositions on a timescale of days [*Munger et al.*, 1998]. The concentration of NO$_y$ is conserved therefore to a larger extent than that for any of its constituent species [*Roberts*, 1995; *Seinfeld and Pandis*, 1998]. Emissions of NO$_x$ provide the only significant source of NO$_y$. Accordingly, in this study we choose to concentrate on measurements of NO$_y$ as the most appropriate surrogate with which to diagnose emissions of NO$_x$.

Table 1. A Priori and A Posteriori Emissions of CO

State Vector Element	A Priori Emissions With Uncertainty	A Posteriori Estimate Using Both TRACE-P and Station Data		A Posteriori Estimate Using TRACE-P Data Only[c]	
		Emissions With Uncertainty[a]	Percent Change[b]	Emissions With Uncertainty[a]	Percent Change[b]
Rest of world[d]	2074 ± 362	2234 ± 20	+8%	2264 ± 20	+9%
SE Asia	127 ± 74	64 ± 3.9	−50%	66 ± 4	−48%
South China[e]	25 ± 15	47 ± 2.0	+88%	36 ± 3.0	44%
Central China	23 ± 18	41 ± 1.5	+75%	73 ± 2.2	38%
North China	30 ± 23	38 ± 2.0	+24%	73 ± 2.2	38%
China total[f]	119 ± 24	170 ± 3.2	+43%	153 ± 3.7	29%

[a]Emissions are given in Tg CO/yr. Uncertainties are reported as either 1-σ value from $\hat{S}$ or the range of solutions from different sensitivity studies, summarized in Figure 14, whichever is the largest.

[b]Percentage change of a posteriori emissions with respect to a priori emissions.

[c]Inversion results using only TRACE-P aircraft observations of CO.

[d]"Rest of world" includes emissions from India, Japan, Korea, northeast China, west China, and secondary CO sources from methane oxidation and biogenic NMVOCs, in addition to regions geographically outside Asia.

[e]"South China" includes emissions from central-south China and southeast China.

[f]"China total" includes emissions from northeast China and west China that are not listed in the table but included in "rest of world."

[8] CO and NO$_x$ are produced primarily by combustion but with different signatures in terms of the relative strength of their emissions depending on the nature of the combustion process. Combustion of biofuels (including open field burning of biomass) accounts for about 45% of CO emissions in China, but for only about 12% of emissions of NO$_x$, reflecting presumably the relatively low temperatures and low efficiency for combustion under these conditions [*Streets et al.*, 2003]. High-temperature combustion processes, associated for example with the transportation sector and industrial boilers, provide important sources of both CO and NO$_x$. Emissions of CO and NO$_x$ in the bottom-up approach are obtained by applying species-specific emission factors to a common base of activity data. A study of the variation of CO relative to NO$_y$ should provide important additional information therefore on the sources of these species over and above what we might expect to learn from a study of the species separately. For example, if we were to find that the emission inventory provided a satisfactory representation of NO$_y$ but an underestimate of CO, we might be tempted to attribute the discrepancy to an underestimate of the importance of contribution from the combustion of biofuel.

[9] We begin by using the nested-grid CTM in the forward model [*Y. Wang et al.*, 2004] to examine the consistency of the bottom-up emission inventory with results obtained from the TRACE-P aircraft mission and the Chinese surface stations over the period of January to April 2001. The forward model, the a priori emissions and the observational data are discussed in section 2. A Bayesian approach to linear inverse analysis [*Rodgers*, 2000; *Palmer et al.*, 2003] is introduced in section 3 and is used to optimize emissions of CO and NO$_x$ consistent with constraints imposed by the combination of the aircraft and station data. The resulting a posteriori representation of emissions is discussed in section 4, which includes an analysis of the sensitivity of the inversion results to assumptions inherent in the inversion approach. The analysis suggests that emissions of both CO and NO$_x$ are underrepresented in the bottom-up inventory. The pattern of the discrepancies observed for the combination of CO and NO$_y$ is exploited in section 5 to explore possible explanations for this disagreement. The a posteriori emis-

sions are adopted and employed in the forward model to a detailed analysis of the surface data in section 6. Summary remarks are presented in section 7.

2. A Priori Emissions, the Forward Model, and Observations

2.1. A Priori Emissions

[10] A priori emissions of CO, NO$_x$ and nonmethane volatile organic compounds (NMVOCs) resulting from combustion of fossil and biofuels over Asia were taken from *Streets et al.* [2003]. For emissions associated with fossil and biofuels over the rest of the world we adopted inventories reported by *Bey et al.* [2001] and *Yevich and Logan* [2003], respectively. Emissions from biomass burning were included on a monthly, climatological mean, basis following the analysis of *Duncan et al.* [2003], with an exception for CO for which we used daily data for the period February–April 2001 provided by *Heald et al.* [2003]. This daily resolved emission inventory was obtained by applying daily variability constrained by fire-count data from AVHRR satellite to the biomass-burning emission inventory of CO from *Duncan et al.* [2003]. Tables 1 and 2 provide summaries of annual a priori emissions of CO and NO$_x$ for different geographical regions, with spatial distributions presented in Figures 1a and 2a for CO and NO$_x$, respectively.

[11] We allowed for seasonal variations in CO emissions associated with fossil fuel and biofuel use in subregions of China, as recommended by *Streets et al.* [2003]. Table 3 lists scaling factors applied to annual mean data for the four-month simulation period, January to April 2001. The seasonal dependence was obtained by assuming a certain temperature dependence for the number of daily operation hours for stoves. Seasonality in NO$_x$ emissions from fossil and biofuels, reported only on national level for China, is less distinct than that for CO [*Streets et al.*, 2003]. Accordingly, annual average results for NO$_x$ emissions quoted by *Streets et al.* [2003] were assumed to apply on a year-round basis.

2.2. Forward Model

[12] The nested-grid GEOS-CHEM model developed by *Y. Wang et al.* [2004] was used to establish the relationship

Table 2. A Priori and A Posteriori Emissions of NO$_x$

State Vector Element	A Priori Emissions With Uncertainty	A Posteriori Estimate Using Both TRACE-P and Station Data		A Posteriori Estimate If V_d of NO$_y$ Species Decreased by 50%[c]	
		Emissions With Uncertainty[a]	Percent Change[b]	Emissions With Uncertainty[a]	Percent Change[b]
Rest of world[d]	70 ± 23	70 ± 3.9	0	71 ± 3.9	−1%
SE Asia	7.3 ± 3.6	4.1 ± 1.6	−43%	4.6 ± 1.6	−37%
South China[e]	2.7 ± 0.9	3.9 ± 0.2	47%	3.5 ± 0.2	33%
Central China	2.2 ± 0.7	6.3 ± 0.2	189%	5.4 ± 0.2	145%
China total[f]	11.2 ± 2.4	16.5 ± 0.5	47%	13.1 ± 0.5	17%

[a]Emissions are given in Tg NO$_2$/yr. Uncertainties are reported as either 1-σ value from $\hat{S}$ or the range of solutions from different sensitivity studies, summarized in Figure 15, whichever is the largest.

[b]Percentage change of a posteriori emissions with respect to a priori emissions.

[c]Inversion results using the forward model simulation when the dry deposition velocity of individual NO$_y$ species is decreased by 50%.

[d]"Rest of world" includes emissions from India, Japan, Korea, northeast China, west China, north China, and regions geographically outside Asia.

[e]"South China" includes emissions from central-south China and southeast China.

[f]"China total" includes emissions from north China, northeast China, and west China that are not listed in the table but included in "rest of world."

between emissions and atmospheric concentrations. The GEOS-CHEM model is driven by the GEOS assimilated meteorological data from the NASA Global Modeling and Assimilation Office (GMAO). The nested grid formation adopted here is based on GEOS-CHEM v5.08 (http://www-as.harvard.edu/chemistry/trop/geos). The model structure involves a window with a uniform horizontal resolution of $1° \times 1°$ embedded in a low-resolution ($4° \times 5°$) global background. The high-resolution regional simulation is coupled dynamically to the low-resolution global model through lateral boundary conditions. For the present study, the nested domain is set at $70°–150°E$ and $11°S$ to $55°N$ and includes all of China, its neighboring countries, and a significant portion of the northwestern Pacific as illustrated

in Figure 3. Compared to the low-resolution global model, the higher-resolution model allows for more efficient, advection-related, ventilation of the lower atmosphere reflecting the significance of localized regions of intense upward motion not resolved in a coarser-resolution simulation [*Y. Wang et al.*, 2004].

[13] Model transport has been described in detail by *Y. Wang et al.* [2004]. The depth of the mixing layer plays a key role in determining concentrations of trace species near the surface. Mixing depths are diagnosed by the GEOS data in terms of the pressure level at which the turbulent kinetic energy is equal to 10% of the value in the surface layer [*Allen et al.*, 1996]. *Fiore et al.* [2002] showed that mixing depths over the United States simulated by the GEOS data
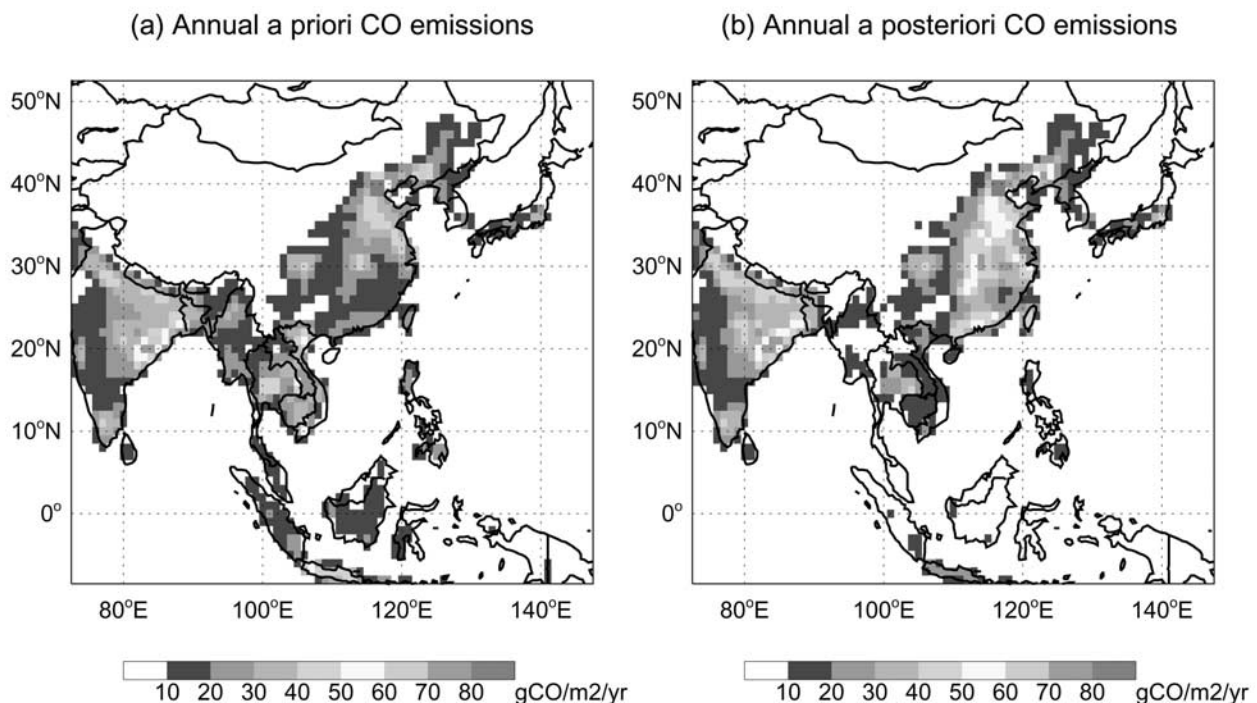

Figure 1. (a) A priori and (b) a posteriori annual emissions of CO for Asia. A posteriori emissions are from the inverse analysis in which both TRACE-P and surface data are employed. See color version of this figure at back of this issue.
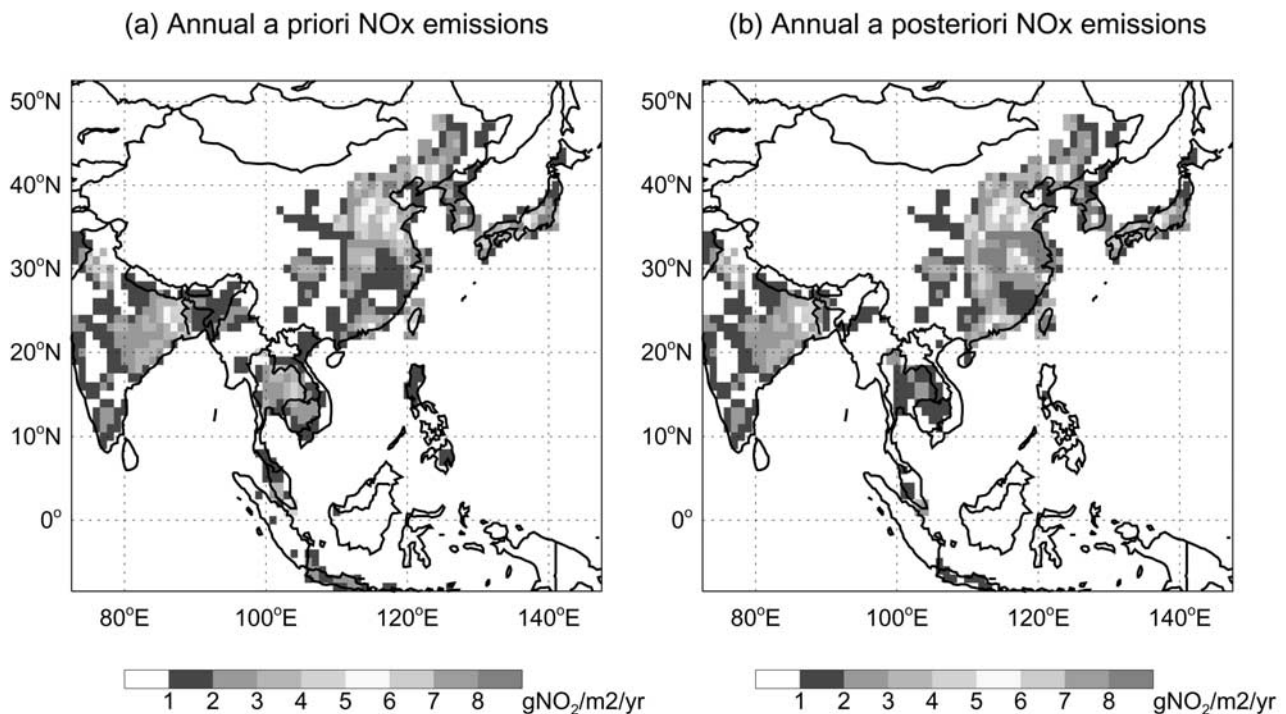
(a) Annual a priori NOx emissions

(b) Annual a posteriori NOx emissions

Figure 2. Same as Figure 1, but for NO$_x$ emissions. See color version of this figure at back of this issue.

are consistent with field measurements and general climatology. As far as we know, there are no direct measurements of mixing depths available to test the model over China except for Hong Kong. The Hong Kong Observatory (HKO) measures afternoon maximum mixing depths on a daily basis at King's Park in Hong Kong. Figure 4a compares the mixing depths measured by the HKO with model predictions for the grid box that includes King's Park. Simulated mixing depths are on average 23% lower than observed values.

[14] The discrepancy may be attributed to the inability of the $1° \times 1°$ model to resolve the land-sea boundary over coastal regions. As depicted in Figure 4b, a significant portion of the Hong Kong grid box in the model is occupied by ocean where afternoon mixing depths are generally lower than over land reflecting differences in land/sea surface heating. As a consequence of this particular grid configuration, mixing depths in the model on average should tend to be lower than would be implied by observations over land. However, we do not believe that this should introduce any significant bias in terms of our interpretation of the measurements at Hok Tsui, for two reasons. First, the surface site at Hok Tsui is located on the edge of a landmass with 240 degrees of ocean (Figure 4b; section 2.4). One might expect the mixing depth at Hok Tsui consequently to be less than that at King's Park reflecting a greater marine influence. Second, the combination of land and ocean in a particular grid element should result inevitably in an underestimate of emissions over the unresolved land portion of the grid. The combination of a mixing layer that may be too shallow and emissions that may be too low should have compensating effects in terms of their effect on the simulation of concentrations at the surface.

[15] For other environments for which measurements of mixing depths are unavailable, we assume that the model provides a realistic simulation of the daytime mixing layer depth. The model, however, is incapable of simulating the shallow nocturnal layers expected to form at night in that the first layer of the model extends typically to a height of about 100 m ($\sigma = 0.998$) above the surface. Accordingly, we choose in the subsequent analysis not to include nighttime measurements distinguished by particularly high concentrations for the gases of interest.

[16] The model includes 80 chemical species and over 300 reactions appropriate for a detailed description of tropospheric ozone-NO$_x$-NMVOC chemistry [*Wang et al.*, 1998]. For consistency with the NO$_y$ simulation, CO was treated concurrently with other species, a procedure different from the offline CO-only simulation adopted by *Y. Wang et al.* [2004]. Differences in CO concentrations between the two cases are small, however, over Asia, consistent with our previous assertion that the distribution of CO over east Asia in spring is determined primarily by long-range transport

Table 3. Seasonality Applied for CO Emissions From Fossil Fuel and Biofuel in China[a]

Regions[b]	January	February	March	April
Northeast China	1.4	1.2	1.2	0.9
North China	1.4	1.2	1.2	0.9
Central China	1.75	1.4	1	0.85
Central south China	1.45	1.14	1.1	0.9
Southeast China	1.45	1.14	1.1	0.9

[a]Data are taken from *Streets et al.* [2003]. The annual mean values are set to be 1.

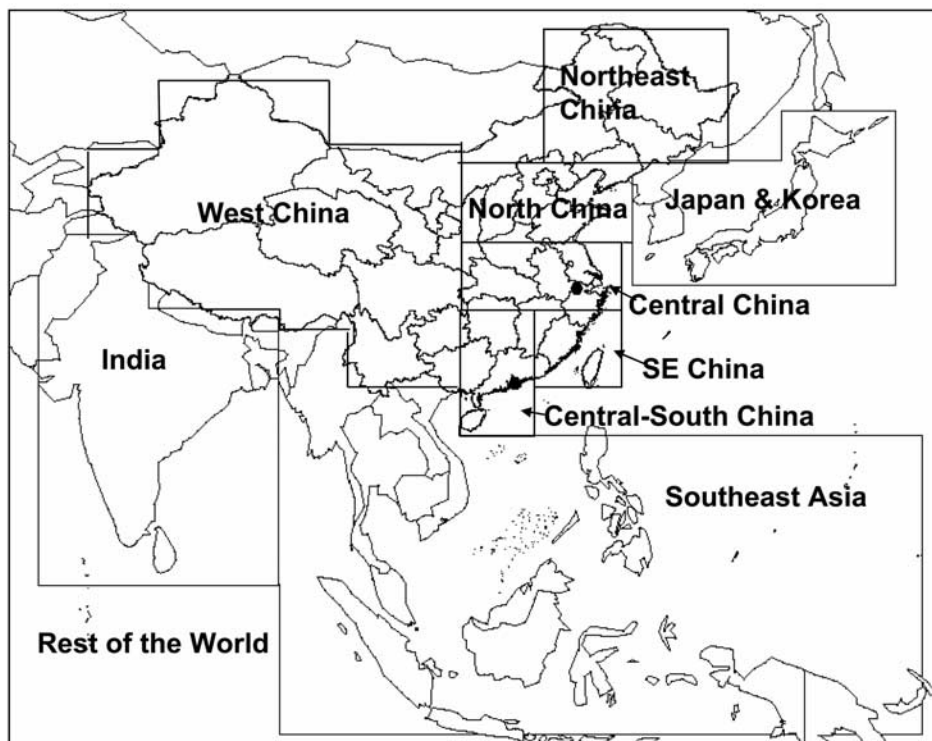[b]Geographical definition of the regions is shown in Figure 3.

Figure 3. Domain of the higher-resolution ($1° \times 1°$) nested window ($70°-150°$E and $11°$S to $55°$N) and tagged source regions. The two black circles indicate locations of the two Chinese surface stations, Hong Kong and Lin An.

and by the spatial pattern of sources [*Y. Wang et al.*, 2004]. The gas-phase chemistry for NO$_y$ follows *DeMore et al.* [1997] and *Horowitz et al.* [1998]. Hydrolysis of N$_2$O$_5$ on aerosols was included in the model with different reaction probabilities (γ) for different types of aerosols (M. J. Evans, N$_2$O$_5$ hydrolysis on aerosol, in "The GEOS-CHEM Chemical Mechanism, Version 5-07-8," 2003, available at http://www-as.harvard.edu/chemistry/trop/geos/documentation/ chem_mech/geoschem_mech.pdf). Uptake of NO$_3$ and NO$_2$ in aerosols was treated using the formalism described by *Martin et al.* [2003]. No attempt was made to distinguish between nitrate in the gas and particulate phases. Both observed and simulated nitrate concentrations shown in this work refer to the combination of gas-phase nitric acid and aerosol nitrate, i.e., the amount of total inorganic nitrate produced from oxidation of NO$_x$.
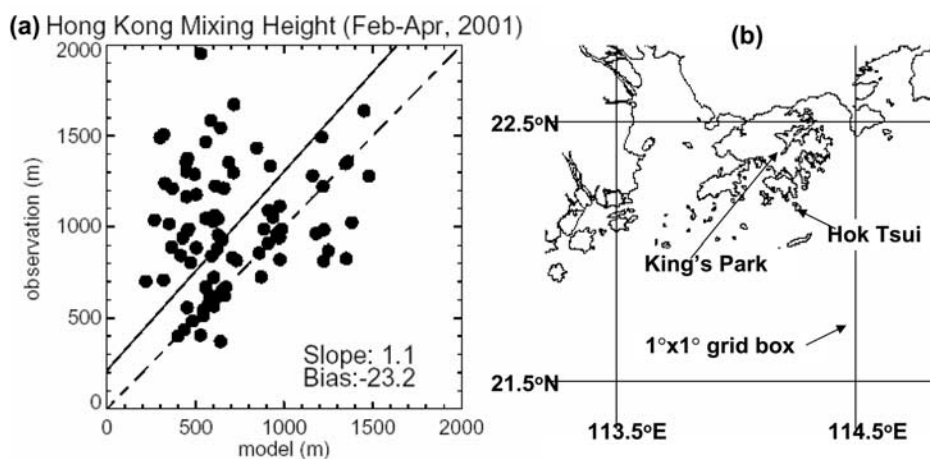

Figure 4. (a) Scatterplot of observed daily maximum mixing height versus model predictions for the Hong Kong site. Data shown are for the period February–April 2001. Observations were made at King's Park in Hong Kong by Hong Kong Observatory. Model predictions are $1° \times 1°$ grid box averages. (b) Locations of King's Park and Hok Tsui (the measurement site) in a $1° \times 1°$ grid box of the model.

[17] Dry deposition of species was computed using a standard resistance-in-series model based on the original formulation of *Wesely* [1989] with a number of enhancements described by *Wang et al.* [1998]. Component species of NO$_y$ subject to dry deposition include NO$_2$, HNO$_3$ (composite gas- and aerosol-phase nitrate), N$_2$O$_5$, PAN and other organic nitrate. Dry deposition velocities were calculated locally using GEOS data for surface momentum and sensible heat fluxes, temperature, and solar radiation. Wet deposition (applied to HNO$_3$) accounted for scavenging in convective updrafts, convective anvils, and for removal by large-scale precipitation [*Liu et al.*, 2001].

[18] Since deposition rates differ for different NO$_y$ species (HNO$_3$, for example, is deposited much faster than NO$_2$), errors either in model chemistry or in relative rates for deposition (wet or dry) can lead to errors in concentrations computed for NO$_y$ and could impact thus our later analysis of emissions. One way to evaluate the model is to compare simulated contributions of component species to NO$_y$ with observations. We performed this comparison for TRACE-P aircraft observations (results shown in section 2.3) and found no evidence of systematic bias.

[19] To determine the relationship between sources and concentrations, emissions from 10 geographical regions were labeled (Figure 3) and their impacts on model fields were determined by analyzing differences between standard and sensitivity simulations in which emissions were eliminated sequentially from each region and sufficient time (2 months) was allowed to eliminate effects of model initialization. The source regions selected for this purpose were Japan and Korea; Southeast Asia; India; west China; northeast China; north China; central China; central-south China; Southeast China; and the rest of the world, as indicated in Figure 3. The high-resolution window approach allows us to differentiate contributions from individual subregions of China on a much finer scale than was possible previously [*Palmer et al.*, 2003]. The influence of the rest of the world was incorporated in the present formulation through its impact on the time varying boundary conditions imposed on the window region using results from the lower resolution global model. Secondary sources of CO associated with oxidation of volatile organic compounds (VOC) species such as CH$_4$ and isoprene are included for convenience under the category "rest of the world."

2.3. TRACE-P Aircraft Observations of CO and NO$_y$

[20] The TRACE-P mission was conducted over the period March–April 2001 with an objective to characterize the outflow of chemicals from Asia in spring [*Jacob et al.*, 2003]. Two aircraft (DC-8 and P3-B) sampled a wide range of locations over the western Pacific from bases in Hong Kong and Japan (Figure 5 shows flight tracks). One-minute average data west of 150°E were adopted for purposes of this study. Since coarse-mode aerosol nitrates were not measured on P3-B flights and since the model simulates only concentrations of total nitrate without regard for phase partitioning, we chose to restrict our analysis to NO$_y$ measurements carried out on the DC-8 flights. In the absence of direct measurements of NO$_y$ [*Talbot et al.*, 2003], we assume that NO$_y$ may be represented by the sum of NO, NO$_2$, PAN, HNO$_3$, aerosol nitrate, and C1–C5 alkyl nitrates. For consistency, these species were sampled
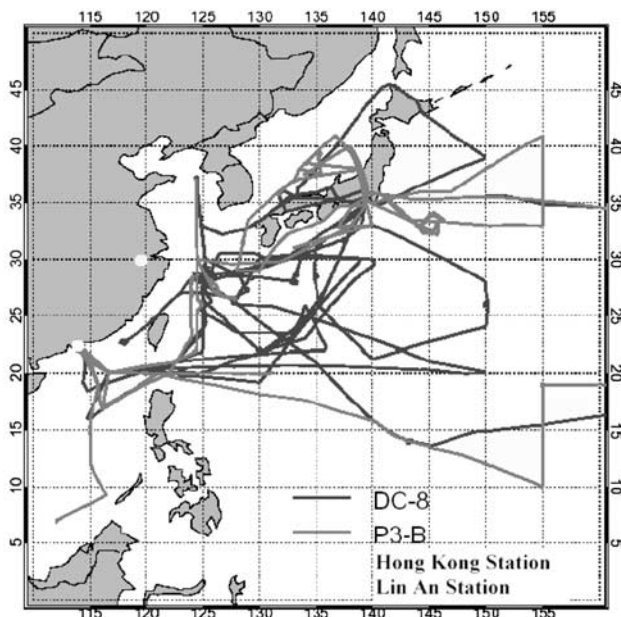

Figure 5. TRACE-P flight tracks and locations of the two Chinese stations. See color version of this figure at back of this issue.

from model fields along flight tracks and their sum is taken to represent the concentration of NO$_y$.

[21] *Y. Wang et al.* [2004] reported an extensive comparison of concentrations of CO obtained using the forward model with results from the TRACE-P aircraft mission. The model was shown to capture satisfactorily observed spatial variances of CO concentrations, but to underestimate concentrations of CO for the boundary layer north 20°N where anthropogenic emissions from China are expected to dominate. The magnitude of the underestimate increases with latitude, reaching as much as 100 ppb around 35°N. An overall comparison of simulated CO and NO$_y$ with observations is presented in Figures 6a and 6b. The data are displayed here as functions of altitude. The observational results are indicated by red circles with red horizontal lines denoting means and 1-σ standard deviations, respectively. Model results obtained using a priori emissions (black lines) are presented in terms of means evaluated for specific flight times and conditions. The model satisfactorily captures the observed vertical gradient, but tends to underestimate concentrations observed in the boundary layer (below 2 km). Using a priori emissions, the model underestimates the ensemble of TRACE-P CO observations by about 20 ppb, with the discrepancy, about 40 ppb, greatest in the boundary layer (Figure 6a). Model results for NO$_y$ are lower than observation by about 30% on average (Figure 6b).

[22] Ratios of component NO$_y$ species to total NO$_y$ are presented in Figure 7. Here, observations are indicated in red with model results in black. By comparing ratios, we effectively eliminate the influence of biases in emissions and focus mainly on possible errors in the model treatment of chemistry and deposition. The comparisons displayed in Figure 7 indicate that bias in the model is minimal below 6 km lending confidence to the treatment of chemistry and
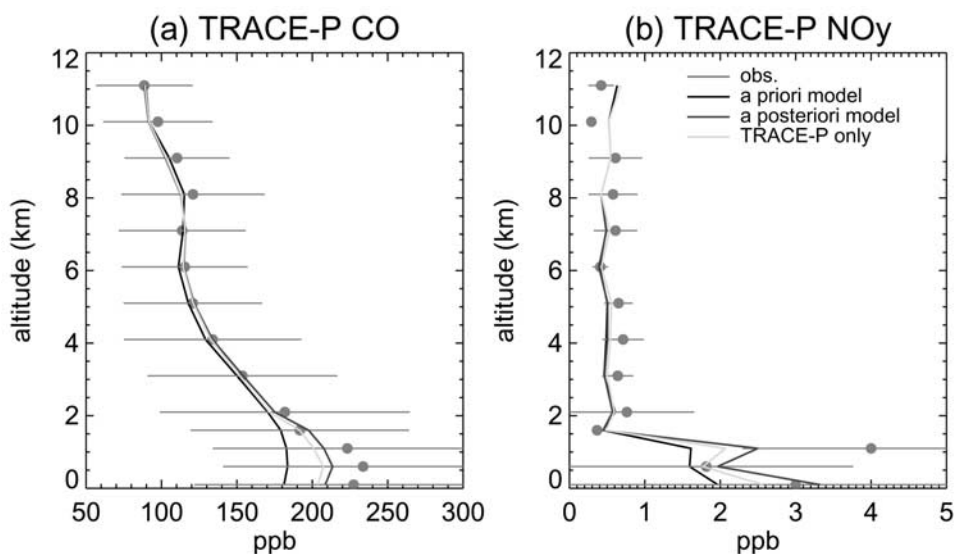
Figure 6. Comparison between model simulations and TRACE-P observations of (a) CO and (b) NO$_y$. The data are shown as a function of altitude. Red circles are mean concentrations of observations, and red horizontal lines indicate 1-σ values around the mean. Black lines are mean values of simulated concentrations using a priori emissions. Blue lines are mean model results using a posteriori emissions from the inverse analysis in which both TRACE-P and the surface observations are employed. Green lines are mean model results using a posteriori emissions for the "TRACE-P only" case. See color version of this figure at back of this issue.

relative deposition rates for individual NO$_y$ species in the model. The major component of NO$_y$ below 2 km is nitrate (both gas and aerosol phases), accounting for over 60% of total NO$_y$, followed by NO$_x$ (~15%) and PAN (~10%). The model tends to underestimate contributions of NO$_x$ to NO$_y$ between 6 and 9 km, compensated by an overestimate of the concentration of nitrates. Fluxes of NO$_y$ from the stratosphere are expected to make a significant contribution to the budget of NO$_y$ in this region. We believe that the discrepancy at higher altitudes may relate to a bias in partitioning stratospheric NO$_y$ fluxes between NO$_x$ and HNO$_3$, rather than to possible errors in model chemistry for the troposphere. The problems at higher altitude are not expected to affect the inversion analysis since total NO$_y$ concentrations

are simulated satisfactorily by the model even for this region (Figure 6b).

2.4. Surface Observations of CO and NO$_y$

[23] The measurements of CO and NO$_y$ from Hong Kong and Lin An used in this study cover the period from 19 February to 30 April 2001 with a temporal resolution of one hour. The locations of the sites are indicated in Figure 5. The Hong Kong station (Hok Tsui, 22°13′N, 114°15′E, 60 m above sea level) is located on the southeastern tip of Hong Kong Island. It is located in a relatively clean area of Hong Kong, on a cliff with 240 degrees of ocean view stretching from northeast to southwest. Urban areas of Hong Kong are normally downwind with respect to the prevailing east-
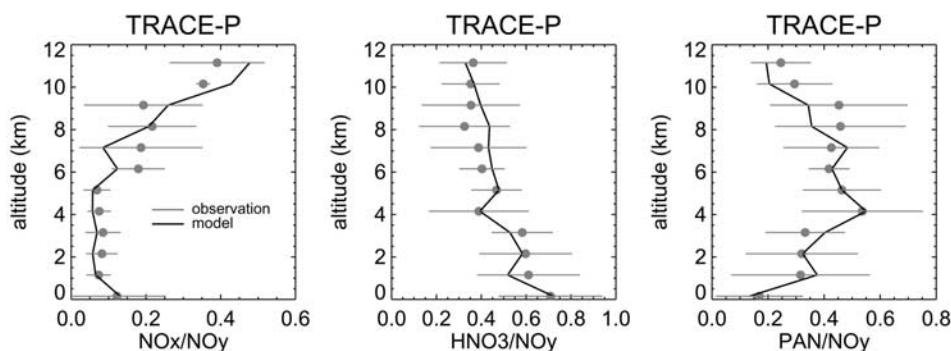

Figure 7. Comparison between simulated and observed (left) NO$_x$/NO$_y$, (middle) HNO$_3$/NO$_y$, and (right) PAN/NO$_y$ ratios made by DC-8 aircrafts in the TRACE-P mission. The data are shown as a function of altitude. Red circles are mean concentrations of observations, and red horizontal lines indicate 1-σ values around the mean. Black lines are mean model results using a priori emissions. Concentrations of HNO$_3$ shown in the middle panel are composite concentrations of gas-phase and aerosol-phase nitrates. See color version of this figure at back of this issue.
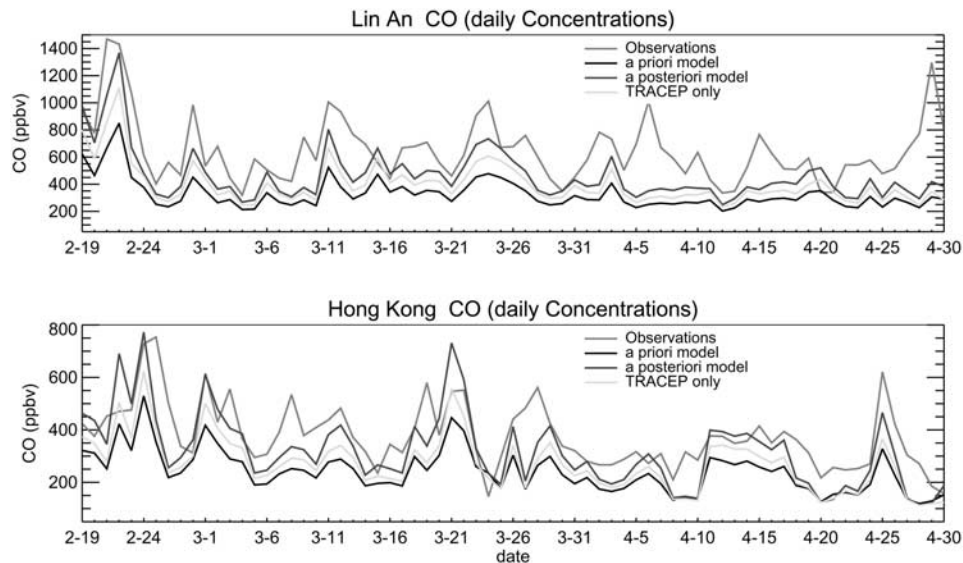
Figure 8. Daily average mixing ratios of observed and modeled CO concentrations at (top) Lin An and (bottom) Hong Kong during 19 February to 30 April 2001. Red lines show observations. Black lines are simulated concentrations using a priori emissions. Blue lines are model results using a posteriori emissions from the inverse analysis in which both TRACE-P and the surface observations are employed. Green lines are mean model results using a posteriori emissions for the "TRACE-P only" case. See color version of this figure at back of this issue.

northeast flow in spring, thus this site is not influenced by local sources and observations are more representative of the larger-scale situations. The Lin An site (30°25′N, 119°44′E, 132 m a.s.l.) is located in a hilly agricultural/forested area on the southern edge of the Yangtze River Delta 53 km west and 210 km southeast of the major population centers of Hangzhou and Shanghai, respectively. The township of Lin'an (population: about 50,000) is 10 km to the south. Further details of the two stations and instrumental methods are given by *T. Wang et al.* [2003, 2004].

[24] To compare model results with observation, we sampled concentrations computed for the grid boxes in which the two stations are located. Day to day variations of CO are presented for Lin An and Hong Kong in the top and bottom panels of Figure 8, respectively. Observations are indicated by the red lines, with model results computed using a priori emissions displayed in black. Daily average values for concentrations were obtained by averaging hourly mean values after eliminating measurements judged to be contaminated by local sources of pollution. In making this judgement, we eliminated all nighttime measurements of CO and NO$_y$ for which concentrations fell outside the 87.5 percentile [*Munger et al.*, 1998]. We also selectively removed daytime data on the basis of a concurrent examination of NO and SO$_2$. The model captures well the temporal variability of CO observed both at Hong Kong and Lin An, with correlation coefficients (r) of 0.8 and 0.7, respectively. The bias between model and observation averages -34% (or -133 ppb) for Hong Kong and -47% (-322 ppb) for Lin An. Analogous results for NO$_y$ are presented in Figure 9. As for CO, the model does a satisfactory job in reproducing the temporal variability observed for NO$_y$ (r values of 0.7 and 0.5 for Lin An and Hong Kong, respectively). However, model results for

NO$_y$ are again systematically too low, by a factor of 3 for Lin An and by about 20% for Hong Kong. *Carmichael et al.* [2003] used a regional-scale model with emissions similar to those contained in the a priori inventory employed here and reached a similar conclusion. Their model underestimated concentrations of CO and NO$_y$ for Lin An in March 2001 by factors of 2 and 3, respectively. It is most likely, we believe, that an underestimate of emissions is primarily responsible for the discrepancies observed in both cases.

3. Inverse Model Analysis

[25] We describe in this section the inverse model used to optimize Asian CO and NO$_x$ emissions, with particular emphasis on error specifications. We adopt the framework of the inverse model described by *Palmer et al.* [2003], which employs a Bayesian approach to linear inversion assuming Gaussian statistics [*Rodgers*, 2000].

3.1. Model Framework

[26] The objective of the inverse model is to find the optimal level of emissions consistent with observations and model predictions allowing for relevant uncertainties. This optimization is realized by minimizing a χ^2 cost function $\mathbf{J}(x)$, defined by

$$\mathbf{J}(x) = (\mathbf{y} - \mathbf{Kx})^T \mathbf{S}_\Sigma^{-1} (\mathbf{y} - \mathbf{Kx}) + (\mathbf{x} - \mathbf{x}_a)^T \mathbf{S}_a^{-1} (\mathbf{x} - \mathbf{x}_a), \quad (1)$$

where the observations are represented by the vector $\mathbf{y}$, $\mathbf{x}$ is the state vector specifying the optimal choice of emissions and $\mathbf{x}_a$ is the state vector corresponding to the choice of a priori emissions. The linear relationship between sources and concentrations is expressed in terms
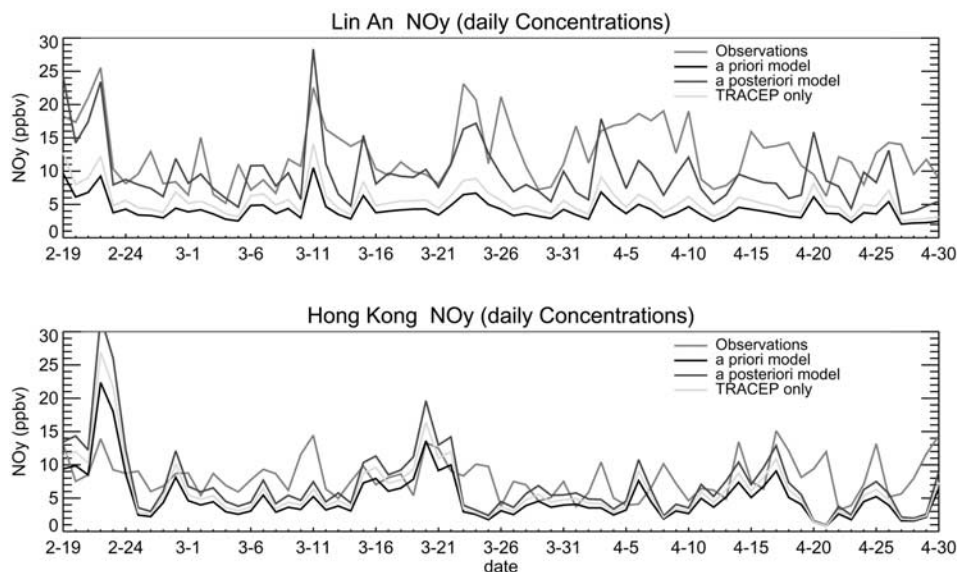
Figure 9. Daily average mixing ratios of observed and modeled NO$_y$ concentrations at (top) Lin An and (bottom) Hong Kong during 19 February to 30 April 2001. Red lines show observations. Black lines are simulated concentrations using a priori emissions. Blue lines are model results using a posteriori emissions from the inverse analysis in which both TRACE-P and the surface observations are employed. Green lines are model results using a posteriori emissions for the "TRACE-P only" case. See color version of this figure at back of this issue.

of the Jacobian matrix **K** with matrix elements computed using the forward model. The error covariance for $\mathbf{x}_a$ is specified in terms of the matrix $\mathbf{S}_a$. The error covariance matrix for the system is defined by $\mathbf{S}_\Sigma$, which allows for contributions due to measurement accuracy, representation error, and errors in the forward model. The first term on the right-hand side of equation (1) describes the mismatch between simulated and observed concentrations weighted by the error of the system. The second term represents constrains imposed by the choice of a priori emissions. A detailed description of the inverse model is given by *Palmer et al.* [2003].

[27] A least squares solution to $\nabla_x(\mathbf{J}(x)) = 0$ yields the optimized state vector $\hat{\mathbf{s}}$ (i.e., a posteriori emissions) and the associated error covariance ($\hat{\mathbf{s}}$ [*Rodgers*, 2000]:

$$\hat{\mathbf{x}} = \mathbf{x}_a + \left(\mathbf{K}^T\mathbf{S}_\Sigma^{-1}\mathbf{K} + \mathbf{S}_a^{-1}\right)^{-1}\mathbf{K}^T\mathbf{S}_\Sigma^{-1}(\mathbf{y} - \mathbf{K}\mathbf{x}_a), \qquad (2)$$

$$\hat{\mathbf{S}} = \left(\mathbf{K}^T\mathbf{S}_\Sigma^1\mathbf{K} + \mathbf{S}_a^{-1}\right)^{-1}. \qquad (3)$$

If errors in the observations are uncorrelated, $\mathbf{S}_\Sigma$ is a diagonal matrix, and equation (2) can be solved sequentially to obtain the a posteriori solution that minimizes the χ^2 cost function.

[28] The a posteriori solution to the inverse problem depends directly on the errors assigned to the observations and to the a priori emissions (equation (2)). The errors for a priori sources from fossil and biofuels in Asia ($\mathbf{S}_a$) were estimated by *Streets et al.* [2003] allowing for the propagation of uncertainties in the "bottom-up" approach. Uncertainties relating to biomass-burning sources and anthropogenic emissions from outside Asia were estimated

following *Palmer et al.* [2003]. The impact of different choices of $\mathbf{S}_a$ and/or $\mathbf{S}_\Sigma$ on a posteriori solutions will be examined in section 4.3.

[29] The inversion is conducted independently for CO and NO$_y$. Concentrations of CO may be assumed to depend linearly on sources since the sink due to OH oxidation is relatively well constrained and chemical coupling with OH is negligible in regions dominated by relatively fresh emissions (1–2 days old for the TRACE-P observations). Emissions of NO$_x$ represent the only significant source of NO$_y$. Chemical transformations between individual NO$_y$ species (including NO$_x$, HNO$_3$, N$_2$O$_5$, NO$_3$, HNO$_4$, PAN, other organic nitrate, and aerosol nitrate) do not impact concentrations of NO$_y$. Discussions in section 2.3 established that there are no systematic biases in the forward model in terms of NO$_y$ chemistry or relative deposition rates. Under the assumption that emission strengths of NO$_x$ should not have a significant impact on the partitioning of NO$_y$ species, we may assume a linear relationship between NO$_x$ sources and atmospheric concentrations of NO$_y$. A simple test of this linearity was implemented by comparing the sum of tagged NO$_y$ tracer concentrations scaled by emission adjustments with NO$_y$ concentrations obtained from model simulations using adjusted NO$_x$ emissions. We verified that results obtained by summing scaled concentrations were identical to those obtained in the model simulation using scaled emissions.

[30] The inverse analysis in this study does not constrain sinks for NO$_y$. Deposition (dry and wet) of NO$_y$ has a nonlinear effect on concentrations of NO$_y$, and its inclusion would complicate the inversion analysis. Under the assumption of minimal bias in the deposition scheme, optimizing sources should effectively optimize also sinks for NO$_y$ since deposition fluxes are coupled closely with concentrations.
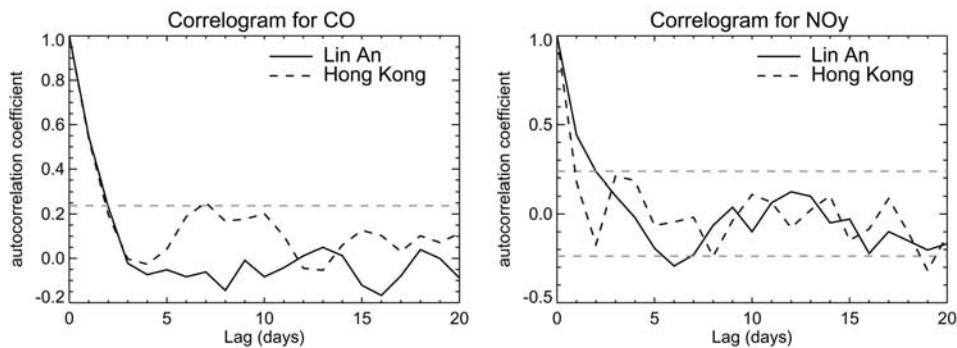
Figure 10. Correlogram (i.e., autocorrelation coefficient R versus time lag) for daily (left) CO and (right) NO$_y$ observations at the two stations (solid line for Lin An and dashed line for Hong Kong). The data shown are between 19 February and 30 April 2001. The grey dashed lines represent 95% confidence limits ($\pm 2/\sqrt{N}$; *Chatfield* [1995]).

In section 4.3, we show that results for the emission inventory obtained using the inversion analysis are insensitive to assumptions made concerning rates for dry and wet deposition.

3.2. Error Specification for Aircraft Observations

[31] We sample 1-hour average model fields along the flight tracks and for the specific flight time. Observations for a particular day are further averaged over a $1° \times 1°$ grid box. In total, in this manner we obtained approximately 2800 and 150 data points for CO and NO$_y$, respectively. We assume that the individual data points are uncorrelated [*Palmer et al.*, 2003]. Error budgets are specified following the procedures described by *Palmer et al.* [2003]. We assumed 2% as the measurement accuracy for CO. The measurement accuracy for NO$_y$ was taken equal to 10%, reflecting larger uncertainties attached to the measurements of individual NO$_y$ species and the summation procedure adopted to convert these measurements to an estimate of total NO$_y$.

[32] Previous work by *Palmer et al.* [2003] used the residual relative error (RRE) to represent the forward model error as a function of altitude and latitude. TRACE-P observations were divided into 11 altitude intervals (evenly distributed from 1 km to 11 km) and 2 latitude bands (north and south of 30°N), and the relative error (RE) between model and observation was calculated for each data interval, i.e., (modeled − measured)/measured. The mean RE is assumed to relate to biases in a priori sources, while the variance about this mean value, or RRE, represents errors associated with the forward model. We apply the same approach here, but use RRE to represent the combination of the forward model error and representation error [*Heald et al.*, 2004]. We found that the sum of the two errors accounts typically for 20% and 30% of observations for CO and NO$_y$, respectively, for TRACE-P.

3.3. Error Specification for Surface Measurements

[33] We assume no covariance for errors between the surface and aircraft observations. Since the surface stations are geographically separated, we assume zero error covariance between the data from these stations. For the individual stations, synoptic weather systems may be expected to introduce error covariances between adjacent observations

and an autocorrelation analysis was applied to daily observations of CO and NO$_y$ to determine the timescale for these synoptic conditions. The autocorrelation analysis gives a measure of correlations between observations separated in time. The normalized autocorrelation coefficient at lag k is defined by

$$r_k = \frac{N}{N-k} \frac{\sum_{t=1}^{N-k}(x_t - \bar{x})(x_{t+k} - \bar{x})}{\sum_{t=1}^{N}(x_t - \bar{x})^2},$$

where N is the number of observations, k is the lag (in days), and $\bar{x}$ is the overall mean [*Chatfield*, 1995]. Figure 10 depicts the correlograms for daily CO and NO$_y$ observations at the two stations. The correlogram shows significant autocorrelation to about 2 days for CO and NO$_y$ for both sites, suggesting that ambient CO and NO$_y$ concentrations at the two sites are subject to the influence of synoptic weather systems on a timescale typically of about 2 days in the springtime. Accordingly, we chose to average observed and simulated concentrations of CO and NO$_y$ over 2-day intervals for both stations. With this procedure, we obtained 70 data points for each species. We assume that the data averaged in this fashion are independent and they are adopted as input to the inversion analysis.

[34] We assume measurement accuracy of 2% and 10% for CO and NO$_y$, respectively [*T. Wang et al.*, 2003]. The total observational error is calculated for each month by applying the RRE approach (section 3.2) to the averaged data set. We assume again that the mean RE reflects biases in a priori sources and the standard deviation of RE, or RRE, represents the sum of the forward model error and representation error. At the Lin An site, RRE increases from 7% in February to 15% in April for CO, and from 7% in February to 11% in April for NO$_y$. At the Hong Kong site, RRE decreases from 14% in February to 8% in April for CO, and from 47% in February to 24% in April for NO$_y$. The magnitude of RRE reflects the ability of the forward model to capture observed variations. Despite fewer observations from the surface data, the associated errors are much less than those for the aircraft observations. Higher RRE for

NO$_y$ at Hong Kong as compared to Lin An is consistent with previous comparisons of correlation coefficient (R) for the two sites (section 2.4).

3.4. Selection of the State Vector

[35] The state vector ($\mathbf{x}$) is constructed solely on the basis of consideration of source regions in Asia. Given that our observations are limited to the Asian region, we do not aim to rigorously constrain sources from other regions of the world. Accordingly emissions from all non-Asian sources are aggregated. Emissions from Korea and Japan are also aggregated as TRACE-P does not provide independent information on the two [*Palmer et al.*, 2003]. Previous inversion studies show that emissions from fossil fuel and biofuel in Asia are colocated to the extent that they cannot be constrained independently [*Kasibhatla et al.*, 2002; *Palmer et al.*, 2003]. Biomass burning in Southeast Asia is also found to be colocated with sources associated with combustion of fossil and biofuels [*Palmer et al.*, 2003]. Emissions from biomass burning in China are small in magnitude and often mixed in with emissions from combustion of fossil and biofuel [*Heald et al.*, 2004].

[36] Previous studies [*Kasibhatla et al.*, 2002; *Palmer et al.*, 2003] used the matrix of averaging kernels ($\mathbf{A} = \mathbf{I} - \hat{\mathbf{s}}\mathbf{s}_a^{-1}$) to examine whether elements of selected state vectors can be constrained by observations. These averaging kernels describe the reduction in the uncertainty attached to the inversion procedure. For a well-constrained source, the averaging kernel should peak at the corresponding state vector element with a value close to 1. Analysis of averaging kernels provides a means to select independent state vectors [*Palmer et al.*, 2003]. However, as the number of observations increases, the a posteriori errors ($\hat{\mathbf{s}}$) are artificially reduced, and the averaging kernels become diagonal and cannot be used to infer information on the correlation of state vector elements. An alternative approach was used by *Heald et al.* [2004], who employed the error correlation matrix (elements r_{ij}) obtained by normalizing $\hat{\mathbf{s}}$ to examine the correlation in the a posteriori solutions:

$$r_{ij} = \frac{\hat{\mathbf{s}}(i,j)}{\sqrt{\hat{\mathbf{s}}(i,i)}\sqrt{\hat{\mathbf{s}}(j,j)}}. \qquad (4)$$

These correlations can be used to identify a situation where large error reduction may be possible for 2 elements (as indicated by peaked averaging kernels) but the resulting estimates may not be independent.

[37] Inspection of the averaging kernels and the error correlation matrix suggest that some of the source regions selected for the forward model simulation (Figure 3) need to be aggregated as neither aircraft nor surface observations can provide independent information on associated emissions. We find that air masses sampled close to Japan and Korea in TRACE-P have passed generally through northeast China and are mixed with air masses originating in Europe. It was found also that the influence of Indian emissions on the observational data considered here is generally small. Emissions from Japan and Korea and emissions from India are aggregated therefore with the rest of world. Emissions from northeast China contribute minimally to the observations at our surface sites and are often mixed with emissions from Europe in the air masses sampled by TRACE-P. The
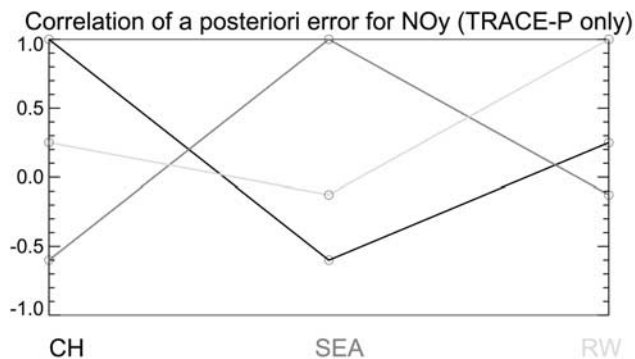

Figure 11. Individual rows of the correlation matrix for the inversion of NO$_y$ sources using only the TRACE-P aircraft data. Different colors distinguish rows of the matrix, with the corresponding columns indicated on the x axis. Lines connect the symbols for clarity and do not have any physical significance. See color version of this figure at back of this issue.

influence of west China is generally weak in both aircraft and surface observations. We choose to lump emissions from northeast and west China with emissions from the rest of the world. The error correlation matrix suggests that sources from central-south China and Southeast China are highly correlated, so we merge these two source regions in a single state vector "south China."

[38] Analysis of the averaging kernels and the error correlation matrix indicate that the aircraft and surface observations have different abilities to independently constrain sources. This is not surprising given the nature of the two data sets. The TRACE-P aircraft campaign sampled a wide range of locations and elevations over the NW Pacific, providing regional snapshots of continental outflows from Asia. They allow in the inversion analysis for constraints on background contributions as well as regional sources, but have limited capability to constrain subregional sources in China, especially for NO$_y$, which has a relatively short lifetime. If only the TRACE-P aircraft observations were used, the inverse model could independently constrain CO emissions from four source regions: Southeast Asia, south China, aggregated north and central China, and the rest of the world. A posteriori CO emissions in the "TRACE-P only" case will be presented in section 4.2. We find that the TRACE-P aircraft observations of NO$_y$ can be used to invert for NO$_x$ emissions from at most three source regions (i.e., Southeast Asia, aggregated Chinese emissions from north, central and south China, and the rest of world), but inspection of the error correlation matrix indicates that a posteriori NO$_x$ emissions in the "TRACE-P only" case may be contaminated by a strong correlation between the aggregated Chinese emissions and Southeast Asia emissions (Figure 11). Therefore we do not conduct a "TRACE-P only" inversion for NO$_x$ emissions. Compared to the aircraft observations, the surface observations made at the two Chinese stations have the advantage of high temporal resolution for fixed locations and high sensitivities to nearby emissions, allowing for constraints on subregional sources in China. Although the two surface sites are not sufficient alone for the inverse analysis as they fail to

provide useful constrains for sources outside China, their roles can be illustrated alternatively by examining the improvements realized as a consequence of integrating them with the aircraft observations. The integrated observational system (i.e., TRACE-P and surface observations) is found to be capable of separating emissions from the following subregions in China which are otherwise impossible with the aircraft observations alone: north, central, and south China for CO emissions and central and south China for NO$_x$.

[39] In summary, the state vector for CO in the integrated observational system has five components: central China (CN. CH), north China (N. CH), south China (S. CH), Southeast Asia (SE. A), and the rest of the world (RW) (Figure 3). The state vector for NO$_x$ has four components: central China (CN. CH), south China (S. CH), Southeast Asia (SE. A), and the rest of the world (RW) (Figure 3). The RW term includes emissions other than listed as an individual state vector. For CO, RW includes also secondary CO sources from methane oxidation and biogenic NMVOCs. Figures 12 and 13 present the averaging kernels (upper panel) and the error correlation matrix (lower panel) for the state vectors of CO and NO$_y$ obtained from analysis of the integrated observations. Distinct peaking of averaging kernels on their own elements of the state vector and small correlation between any of the state vector elements indicate that the integrated observational system is able to separate the selected source regions through inversion and obtain independent top-down constraints for the associated emissions. The difference between the state vector components of CO and NO$_y$ reflect differences in the lifetimes of the two

Figure 13. Same as Figure 12, but for the state vector of NO$_y$ inversion. The four-element state vector for NO$_y$ includes total sources from central China (CN. CH), south China (S. CH), Southeast Asia (SEA), and the rest of the world (RW). See color version of this figure at back of this issue.
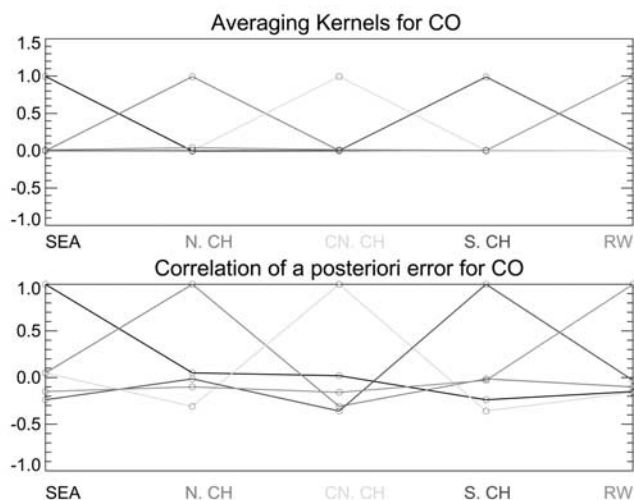

Figure 12. (top) Individual rows of the averaging kernel matrix **A** for the inversion of CO sources and (bottom) individual rows of the error correlation matrix. Different colors distinguish rows of the matrix, with the corresponding columns indicated on the x axis. Lines connect the symbols for clarity and do not have any physical significance. The five-element state vector for CO includes total sources from Southeast Asia (SEA), north China (N. CH), central China (CN. CH), south China (S. CH), and the rest of the world (RW). See color version of this figure at back of this issue.
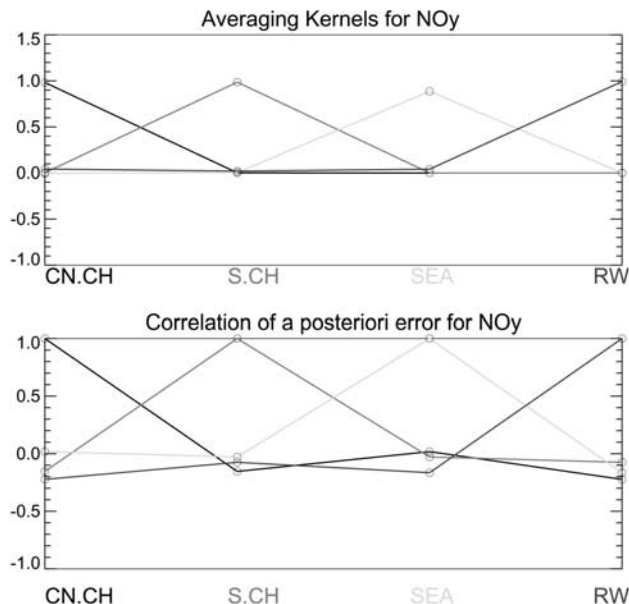
species. Our later discussion (section 5) of the implications for the "bottom-up" emission inventory for China of the a posteriori results obtained for emissions of CO and NO$_x$ in the inversion analysis will focus mainly on the source regions that are consistently defined in the inverse analysis for both CO and NO$_x$, namely south China and central China.

4. A Posteriori Emissions

[40] The a posteriori estimates for emissions and associated uncertainties obtained from our best case scenario in which both the aircraft and station observations are employed (the "integrated" case) are presented in section 4.1. We will argue that use of the a posteriori emissions significantly improves the ability of the forward model to match observations. The role that each of the data sets (aircraft and surface measurements) plays in the inverse analysis is discussed in section 4.2. Different sensitivity studies are conducted in section 4.3 to test whether a posteriori solutions may be judged to be robust.

4.1. A Posteriori Emissions and Comparisons With Observations

[41] A posteriori solutions to the selected state vector using the integrated observational system are summarized in Tables 1 and 2 for CO and NO$_x$, respectively. A priori emissions with uncertainties are shown for comparison. Uncertainties of a posteriori emissions, calculated as 1-σ value from ŝ, are significantly less than a priori values. The value of the cost function (equation (1)) is reduced by 30% from 4060 to 2900 for CO (n = 2600) and by 47% from 509 to 270 for NO$_x$ (n = 230). A posteriori cost functions have

the order of magnitude as the number of observations, indicating a successful inversion [*Palmer et al.*, 2003]. The inversion analysis suggests that emissions from RW should increase by 9% for CO while remaining the same for NO$_x$, as compared to the a priori standard. Given the uncertainties in global OH concentrations as well as uncertainties in emissions from other countries, 9% appears to represent a reasonable adjustment for CO and is comparable to that obtained in other studies [*Palmer et al.*, 2003].

[42] Composite CO emissions for the Asian window region are presented in Figure 1 with the a priori emissions to the left and the a posteriori emissions to the right. The inversion analysis indicates a 50% decrease in a posteriori emissions of CO from Southeast Asia relative to a priori, consistent with conclusions reached in other TRACE-P studies [*Palmer et al.*, 2003; *Heald et al.*, 2004]. This decrease is driven mainly by the overestimate by the model of TRACE-P observations south of 25°N in the middle troposphere where emissions from biomass burning in Southeast Asia appear to dominate [*Y. Wang et al.*, 2004]. Emissions of CO from all source regions in China are increased, with a maximum increase of 88% in south China with a minimum of 24% in north China. Emissions of CO from central China are increased by 75%. The large increase in emissions from central and south China are driven mainly by the need to correct the model underestimate of surface measurements at Lin An station (in central China) and Hong Kong (in south China), reinforced by the model underestimate of TRACE-P observations for the boundary layer between 25°N and 35°N [*Y. Wang et al.*, 2004]. As explained before, the TRACE-P observations and the two ground stations cannot provide independent top-down constraints on CO emissions from west and northeast China and they were aggregated in RW. If CO emissions from these two regions are assumed to be increased by 9% according to the adjustment made to RW, the results suggest that total CO emissions from China should increase to 170 Tg/yr, 43% more than the a priori value of 119 Tg/yr.

[43] Inversion results for NO$_x$ emissions are generally consistent with CO emissions in terms of the sense of the adjustments. Composite NO$_x$ emissions for the Asian window region are presented in Figure 2 with the a priori emissions on the left and the a posteriori emissions on the right. The a posteriori estimate of NO$_x$ emissions from Southeast Asia is decreased by 43% relative to a priori. Emissions of NO$_x$ from central China and south China are increased by 189% and 47% relative to a priori, respectively. These large increases are driven by the need to correct for the model underestimate of concentrations measured at the surface stations, similar to the situation observed for CO. If NO$_x$ emissions from other Chinese regions (i.e., north China, west China, and northeast China) are taken equal to values assumed in the a priori inventory, according to the adjustment made to RW, the analysis suggests that total NO$_x$ emissions from China should be increased by about 47% from an a priori value of 11.2 Tg NO$_2$/yr to 16.5 Tg NO$_2$/yr.

[44] Use of the a posteriori emissions significantly improves the performance of the forward model in simulating both the aircraft and surface observations. Figure 6 presents a comparison of model results using a posteriori emissions (blue lines) with TRACE-P observations (red

lines) and with model results using a priori emissions (black lines). Increasing emissions from China results in a significant increase in concentrations of CO and NO$_y$ simulated for the boundary layer, resulting in a much better match with observations. The a posteriori model results for the two surface stations are displayed as blue lines in Figure 8 (for CO) and in Figure 9 (for NO$_y$), along with observations (red) and a priori model results (black). For CO, the average negative bias of the model is reduced from −34% (or −133 ppb) with a priori emissions to −11% (or −41 ppb) with a posteriori emissions for the Hong Kong station, and from −47% (−322 ppb) to −22% (−158 ppb) for the Lin An station. Similarly, a posteriori emissions of NO$_x$ reduce the model underestimate of NO$_y$ by over 50%. Simulated concentrations with a posteriori emissions are lower than observations at the two stations, due possibly to the aggregation errors discussed below. In this study the spatial distribution of sources within each of the tagged regions was assumed to follow a priori patterns, and the inverse model adjusts only the magnitude of total emissions for each region. This represents a limitation of the inverse method, commonly referred to as the aggregation error. The aggregation error is implicated in the total model error as it is difficult to quantify separately. However, this treatment cannot account for possible biases introduced by the aggregation error. Measurements at the two surface stations may be sensitive to heterogeneity of sources. We conducted several tests in which CO emissions (a posteriori values) were adjusted in several grids surrounding Lin An while keeping the total emission fixed. In one scenario (not necessarily the best), we found a better fit to the observations (bias = −8%). In this case the spatial adjustment assigned higher emissions to rural areas to the west and south of Lin An and spread out emissions along the coast instead of concentrating them over the Shanghai metropolitan region.

4.2. Comparison Between the Two Data Sets

[45] The analysis of section 3.4 indicates that the TRACE-P aircraft observations of CO can provide important constraints on emissions of CO from Southeast Asia, south China, aggregated central and north China, and RW. Analysis of the difference between a posteriori emissions obtained using the TRACE-P observations alone (the "TRACE-P only" case) and the integrated observations incorporating data from both the TRACE-P missions and the Chinese stations (the "integrated" case) offers an opportunity to assess the consistency of the source constraints obtained using two very different data sets. Table 1 lists a posteriori emissions of CO for the "TRACE-P only" case. For individual source regions, the "TRACE-P only" case agrees qualitatively with the integrated case in that both suggest the need for significant enhancements in a priori emissions. A posteriori emissions of CO from Southeast Asia and RW obtained in the "TRACE-P only" case differ by only a few percent from those developed in the "integrated" case, suggesting the dominant role of the aircraft observations in constraining sources from Southeast Asia and RW. A posteriori emissions of CO from the aggregated central and north China in the "TRACE-P only" case amount to 73 Tg/yr, 7% less than the sum of a posteriori emissions calculated separately for central and

north China in the "integrated" case (79 Tg CO/yr). Given that the 7% difference may be attributed to the aggregation error in the "TRACE-P only" case, the aircraft and surface observations are mutually consistent in constraining emissions of CO from central and north China. The surface data allow for a separation of emissions from the two regions while the TRACE-P data help to constrain total emissions from the combined region. The "TRACE-P only" case indicates 23% lower a posteriori emissions from south China (11 Tg/yr less) than the integrated case, and consequently, total Chinese CO emissions are 10% (or 17 Tg/yr) less than for the "TRACE-P only" case. The forward model suggests that on average emissions from south China contribute 13% to CO simulated at either Hong Kong or Lin An, but only 5% to the TRACE-P data south of 30°N in the boundary layer. Thus CO observed at the two surface stations is more sensitive to sources from south China than is the case for the aircraft measurements. Addition of the measurements at the two ground stations to the aircraft record results in higher estimates for a posteriori emissions with lower uncertainties for CO emitted in south China.

[46] The TRACE-P aircraft observations of NO$_y$ cannot provide independent constraints on sources from China and Southeast Asia (section 3.4; Figure 11). An alternative set of "TRACE-P only" NO$_x$ emissions can be obtained by scaling a priori NO$_x$ emissions for each source region using scaling factors derived for CO in the "TRACE-P only" CO case. This simplified method allows only for a qualitative comparison with NO$_x$ emissions inferred in the "integrated" case. A posteriori NO$_x$ emissions for the "TRACE-P only" case exhibit a similar tendency to those obtained in the "integrated" case, with significant increases in emissions implied for central and south China accompanied by a significant reduction in emissions from Southeast Asia.

[47] The consistency between the two data sets is examined further by comparing a posteriori model results obtained using emissions in the "integrated" case with results derived using emissions for the "TRACE-P only" case. The a posteriori NO$_x$ emissions for the "TRACE-P only" were obtained using the simple scaling method described above. Comparisons of model results with the aircraft measurements of CO and NO$_y$ are presented in Figures 6a and 6b, respectively. Results obtained using the a posteriori emissions inferred for the "TRACE-P only" case are indicated by the green lines, while results for the "integrated" study are displayed in blue. Concentrations of CO and NO$_y$ derived for the boundary layer in the "integrated" case are slightly higher than those obtained in the "TRACE-P only" analysis. A posteriori concentrations of CO differ by less than 10% between in the two cases and results from both studies fall within 1 standard deviation of the TRACE-P observations. This suggests a consistency of source constraints obtained for the two cases in terms of their ability to account for the TRACE-P measurements. A comparison with measurements at the surface sites is presented for CO in Figure 8, for NO$_y$ in Figure 9. Concentrations of CO and NO$_y$ obtained in the "integrated" case (blue lines) are significantly higher than those for the "TRACE-P only" case (green lines) and exhibit much better agreement with observation. Concentrations of CO in the "integrated" case are greater than those in the "TRACE-P only" case, typically by about
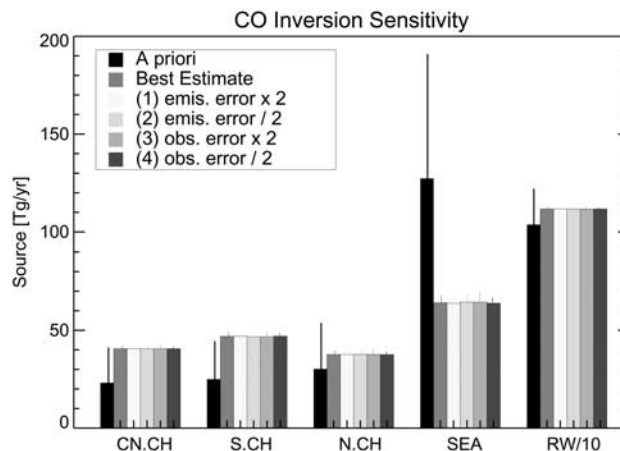

Figure 14. Sensitivity of the calculated a posteriori sources of CO to the error estimates in the inverse model. Vertical bars denote 1-σ value from $\hat{S}$. The range of solutions is summarized in Table 1. Elements in the abscissa are as in Figure 3. See color version of this figure at back of this issue.

15% (50 ppb) with differences extending to more than 100 ppb for some high-CO episodes (e.g., 22 February and 24 March at Lin An, 24 February and 12 March at Hong Kong). Concentrations of NO$_y$ at Lin An in the "integrated" case are significantly higher (by 50%) than for the "TRACE-P only" simulation; differences for Hong Kong are more muted, about 15%. The differences in concentrations of CO and NO$_y$ obtained for the surface sites in the "TRACE-P only" and the "integrated" studies reflect the importance of the additional constraints on near-source emissions imposed by inclusion of the station data in the latter analysis.

4.3. Sensitivity Analysis

[48] A posteriori solutions to the inverse problem depend on the uncertainties assumed for the a priori emissions (S_a) and for the system (S_Σ). We found that doubling and halving either S_a or S_Σ did not significantly affect the a posteriori solutions in the "integrated" case for either CO (Figure 14) or NO$_y$ (Figure 15), suggesting the results obtained in the inversion procedure are relatively robust. The changes in emissions obtained in this sensitivity analysis fell comfortably within the range of uncertainties reported for the a posteriori emissions in section 4.1.

[49] As stated previously, sinks for NO$_y$ are not as well constrained as those for CO in the forward model. We assumed in the inversion analysis that the bias in the simulation of dry and wet deposition of NO$_y$ in the forward model was negligible. The comparison of ratios of component NO$_y$ species to total NO$_y$ between model and aircraft observations discussed in section 2.3 supports the internal consistency of the treatment of deposition for different NO$_y$ species. It is unable, however, to resolve possible errors in the treatment of the loss of NO$_y$. In the absence of specific measurements of NO$_y$ deposition over the study region for the period of interest, we conducted a number of simple tests to examine the extent to which biases in the treatment of deposition by the model could affect conclusions reached
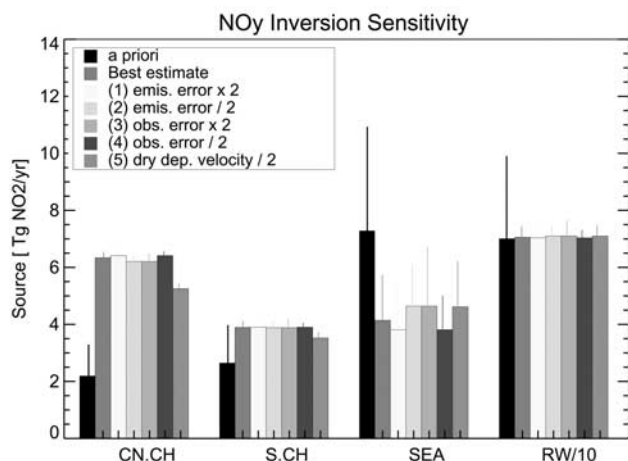
Figure 15. Sensitivity of the calculated a posteriori sources of NO$_y$ to the error estimates in the inverse model. Vertical bars denote 1-σ value from $\hat{S}$. The range of solutions is summarized in Table 2. Elements in the abscissa are as in Figure 3. See color version of this figure at back of this issue.

in the inversion model with respect to emissions. Losses of NO$_y$ associated with wet and dry deposition were reduced in the forward model and emissions of NO$_x$ were recalculated to reflect this adjustment.

[50] Wet deposition was found to play only a minor role in determining NO$_y$ concentrations for the period of interest. Losses of NO$_y$ associated with wet deposition as simulated by the model were appreciably smaller than those for dry deposition, typically by as much as a factor of 2. We explored a range of possible conditions for wet deposition. Concentrations of NO$_y$ were found to vary by less than 1%. We concluded that the inversion results are insensitive to possible errors in the treatment of wet deposition.

[51] The parameter most commonly used to model dry deposition is the deposition velocity (V_d). The GEOS-

CHEM model calculates V_d locally using GEOS meteorological data. Since we are interested here only in the sensitivity of simulated concentrations to dry deposition, we chose to decrease V_d by a uniform factor of 50% for NO$_y$ species subject to dry deposition. Compared to the standard simulation with a priori emissions, a decrease in V_d of this magnitude was found to result in a decrease in the dry deposition flux of NO$_y$ by about 30%, with increases in NO$_y$ concentrations by about 10% for purposes of the TRACE-P comparison, 20% for Lin An, and 10% for Hong Kong (Figure 16). The agreement between model and observed concentrations is not markedly improved despite the reduction in the assumed loss rate. Model concentrations of NO$_y$ are still too low as indicated in Figure 16. An inverse analysis was conducted using the forward model results obtained with decreased V_d (the "V_d decreased" case). A posteriori solutions obtained in this analysis are compared with results from the base case model (unadjusted V_d) in Table 2 and Figure 15. The a posteriori solutions obtained in the "V_d decreased" study are consistent with the base case allowing for relevant uncertainties, except for emissions from central China which are reduced by about 30% in the "V_d decreased" simulation as compared to the base model. However, both cases suggest that NO$_x$ emissions from central China should be increased by more than a factor of 2 with respect to values implied by the bottom-up, a priori, inventory.

5. Implications for the "Bottom-Up" Approach

[52] The a posteriori estimates for CO and NO$_x$ emissions from China derived here are significantly higher than the a priori emissions reported by *Streets et al.* [2003]. The regional distribution of the a posteriori emissions is different also from the a priori (Figures 1 and 2). Errors in the "bottom-up" inventory could be related to problems either with data for sector activities or emission factors or both. It would not be surprising to find that the problems were regionally specific. In this section we try to identify the sources of CO and NO$_x$ from China that are underestimated
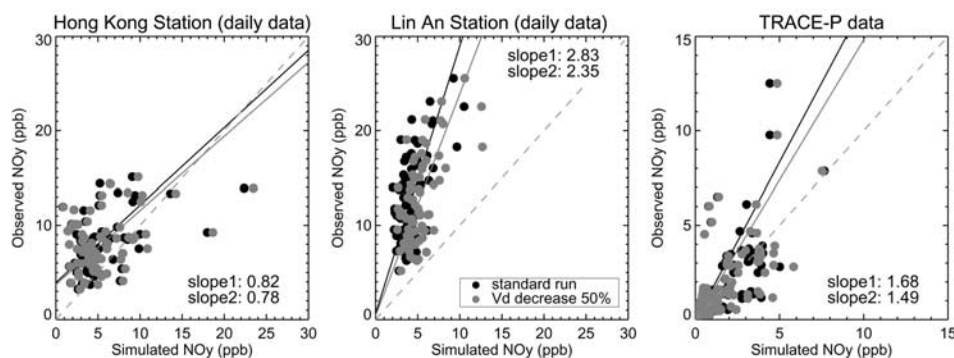

Figure 16. Scatterplots of observed NO$_y$ concentrations versus model results obtained from the standard simulation (black circles) and observed NO$_y$ concentrations versus model results using 50% decreased deposition velocity (V_d) for NO$_y$ species (red circles). Data are separately presented with the Hong Kong station in the left panel, Lin An station in the middle panel, and the TRACE-P mission in the right panel. The slopes between observation and model are also shown: "Slope1" denotes the slope between observation and standard model simulation, and "slope2" denotes that between observation and model simulation with decreased V_d. See color version of this figure at back of this issue.
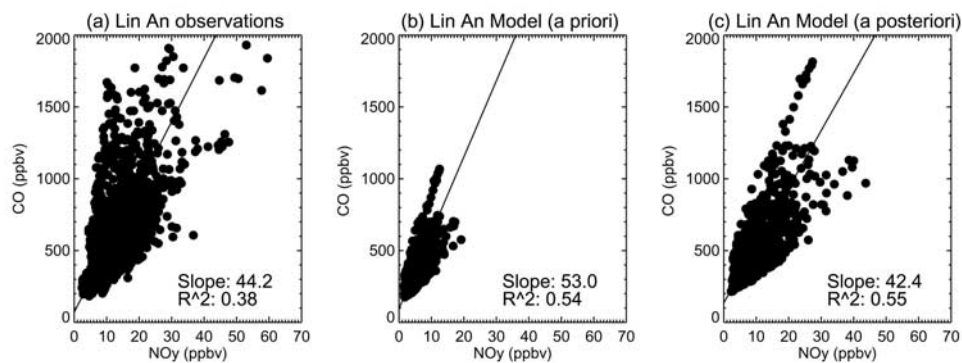
Figure 17. Scatterplots of NO$_y$ versus CO during 19 February to 30 April 2001 at Lin An. Data are shown for (a) hourly observations, (b) hourly model output using a priori emissions, and (c) model output using a posteriori emissions. The correlation coefficient (R) and slope of linear regression are shown for each data set.

in the "bottom-up" approach. Since CO and NO$_x$ have distinct source signatures for different types of combustions, a simultaneous and consistent examination of both species allows for additional constrains on emissions from certain fuel types (e.g., fossil fuel or biofuel).

5.1. Previous Studies

[53] Several studies have commented on possible sources of CO from China that might be underrepresented in the inventory of *Streets et al.* [2003]. *Carmichael et al.* [2003] found that their regional model significantly underestimated both TRACE-P observations over the Yellow Sea and surface observations at Lin An. They attributed the discrepancies to an underestimate of CO emissions from domestic coal burning in central China, indicating that emissions from the domestic sector would have to be increased by a factor of 3–5 to reconcile their model results with observations. However, coal is not the favored residential fuel in the Yangtze Delta Region [*T. Wang et al.*, 2004]. Ambient measurements at Lin An by *T. Wang et al.* [2002, 2004] failed to show a correlation between CO and the distinctive tracer of coal burning, SO$_2$. *Suntharalingam et al.* [2004] suggested that unaccounted emissions of CO from heavily polluting power plants could offer another possible explanation, but concluded that this source alone could not account for an underestimate as large as 54% as suggested by the inverse study of *Palmer et al.* [2003]. *Russo et al.* [2003] found that ratios NO$_y$/SO$_2$ measured during TRACE-P were comparable to those implied by the inventory of *Streets et al.* [2003] and concluded consequently that the inventory should provide a credible representation of NO$_x$ sources from Asia. It is noteworthy that emissions of both NO$_x$ and SO$_2$ are dominated by the industrial and power generation sectors. For example, the power generation sector is responsible for 50% of SO$_2$ emissions and 40% of NO$_x$ emissions in China according to the *Streets et al.* [2003] analysis. As a consequence, the ratio of NO$_y$ to SO$_2$ is relatively insensitive to errors in activity reporting for these sectors, although it can provide a useful check on the internal consistency of emission factors of NO$_x$ and SO$_2$ for the two sectors.

[54] *T. Wang et al.* [2002, 2004] found that measurement derived CO/NO$_y$ ratios at Lin An were about 3 times higher

than the emission-based ratios CO/NO$_x$ implied for the study region by *Streets et al.* [2003]. They suggested that sources contributing significant quantities of CO but relatively little NO$_x$, such as open biomass burning and combustion of biofuels, may have been underrepresented in the *Streets et al.* [2003] inventory. Their analysis assumed that only a small portion of NO$_x$ emitted was converted to HNO$_3$ and lost subsequently by deposition before reaching the measurement site in winter and spring, so that NO$_y$ concentrations could be used as a surrogate for NO$_x$ emissions. Their argument was supported by a low fraction of fine nitrate (PM2.5) in NO$_y$ (nitrate/NO$_y$ = 0.14 ± 0.06) and other indicators for the extent of atmospheric processing measured at Lin An [*T. Wang et al.*, 2004], while our model suggests that nitrate (composite gas phase and aerosol phase of all sizes) represents about 30% of NO$_y$ at Lin An. A direct comparison between measured and simulated contributions of nitrate to NO$_y$ cannot be conducted since coarse mode nitrates were not measured at Lin An. Our model suggests that heterogeneous reactions (hydrolysis of N$_2$O$_5$ in aerosols for example) play a larger role than gas phase reactions in converting NO$_x$ to HNO$_3$ for the period of interest. The rate of gas-phase reactions is expected to be slow under low temperature and reduced sunlight in winter, while the rate of N$_2$O$_5$ hydrolysis increases with decreasing temperature [*DeMore et al.*, 1997]. Clear evidence exists from field observations that hydrolysis of N$_2$O$_5$ in aerosols provides a major sink for atmospheric NO$_x$, especially in winter and at night [*Jacob*, 2000]. Allowing for heterogeneous NO$_x$ chemistry, our model with a priori emissions predicts CO/NO$_y$ ratios at Lin An that are only 20% higher than observation. The ratio decreases by 15% in the "V_d decreased" case (section 4.3). When a posteriori emissions are used, the simulated CO/NO$_y$ ratio at Lin An (42 mol/mol) is close to observation (44 mol/mol). Concentrations of CO as functions of NO$_y$ are presented in Figure 17, with observations from Lin An displayed in Figure 17a, model simulations with a priori emissions in Figure 17b, and model simulations with a posteriori emissions in Figure 17c. Agreement between model and observation is excellent indicating that the "bottom-up" emission inventory does a better job in representing relative emissions of CO and NO$_x$ from

central China than it does for emission of either species separately.

5.2. Noncombustion Sources of NO$_x$

[55] The inversion analysis suggests that NO$_x$ emissions from central China should be increased by a factor of 3 (or by a factor of 2 if uncertainties in simulating NO$_y$ deposition are considered in the "V_d decreased" case) relative to the a priori inventory. As we shall show in the next section, it is impossible to account for an increase of this magnitude solely on the basis of uncertainties in NO$_x$ sources associated with the combustion of various types of fuels. It is well known that microbial processes in soils and human and animal wastes emit NO$_x$ [Logan, 1983; Lee et al., 1997]. The "bottom-up" inventory of Streets et al. [2003] includes only NO$_x$ sources from combustion processes, i.e., combustion of coal, oil, and biofuel. The GEOS-CHEM model assigns negligible sources of NO$_x$ to soils and to applications of fertilizer in China (less than 1% of combustion sources) on the basis of the empirical algorithm of Yienger and Levy [1995] and does not allow for emissions of NO$_x$ associated with decomposition of organic wastes. These sources were also assumed to be small or zero in other models in support of TRACE-P [e.g., Carmichael et al., 2003; Wild et al., 2003; Zhang et al., 2003]. Given large populations of people and animals and the scale of agricultural practices in China, NO$_x$ emissions from noncombustion processes, especially those associated with the human food chain, may play an important role in the budget of NO$_x$. Here we examine two noncombustion sources of NO$_x$: human and animal waste and fertilizer application.

[56] NO$_x$ (mainly NO) and N$_2$O are emitted as by-products of both nitrification and denitrification. Nitrification is thought to provide the primary source of atmospheric N$_2$O [McElroy, 1980] and both in situ and laboratory measurements indicate a close relationship between production of NO and N$_2$O. The ratio of NO to N$_2$O (mole N/mole N) is typically greater than 1, ranging from 1.15 to 22 [Lipschultz et al., 1981; Slemr and Seiler, 1984; Shepherd et al., 1991]. Yields of NO and N$_2$O increase with decreasing oxygen levels and so also does the ratio of NO/N$_2$O. Under low-oxygen conditions, the ratio may be as large as 5 or even higher. We attempt here to estimate the magnitude of microbially related emissions of NO using the more extensive database that exists for N$_2$O.

[57] Emissions of N$_2$O associated from the disposal of nitrogen in human and animal waste may be estimated by applying a yield for N as N$_2$O produced by nitrification relative to the total nitrogen content of the waste. Human populations in the developed world consume and excrete N at an annual average per capita rate of about 5.4 kg N/yr [National Research Council Committee on Nitrate Accumulation, 1972]. A somewhat lower value, 4 kg N/yr, is adopted for central China. For excretion rates of N contributed by different animal types we adopt data recommended by Intergovernmental Panel on Climate Change (IPCC) [1996] for Asia. Using official statistics on human and animal populations [National Bureau of Statistics of China (NBS), 2002], we estimate that human and animal waste was responsible for a nitrogen source of 7.9 Tg N/yr for central China in 2001, of which 80% was contributed by animal waste. We tentatively assign an average value of 2% for the

yield of N$_2$O associated with the disposal of human and animal waste in central China. This choice was made on the grounds that O$_2$ concentrations are likely to be low in environments receiving large inputs of concentrated animal waste and that they are likely also to be depressed under conditions applying to disposal of human waste in the developing world. Yields of this magnitude and higher (approaching 5%) were observed in 1977 under low-flow, low-oxygen conditions in a region of the Potomac River receiving large inputs of N as NH$_4^+$ from the sewage treatment plant at Blue Plains serving Washington, D. C. [McElroy et al., 1978]. Czepiel et al. [1996], on the basis of enclosure measurements, reported a mass-based emission factor of 0.5 g of N$_2$O (dry kg)$^{-1}$ for composted livestock waste with a nitrogen content of 1.5 dry wt%, corresponding to a yield of 2% yield for N as N$_2$O. IPCC [1996] recommends a yield of 2% for pasture ranges and paddocks, where manure is left "as is" on fields. A yield of 2% would imply a source of N$_2$O from waste disposal of 0.15 Tg N/yr for central China. If we assume a ratio NO/N$_2$O ratio of 3, a value in the midrange of results reported in the literature for low-oxygen conditions, NO$_x$ emissions from waste disposal would amount to 0.47 Tg N/yr for 2001 in central China, or 1.6 Tg NO$_2$/yr, corresponding to 73% of a priori NO$_x$ emissions associated with combustion in the inventory developed by Streets et al. [2003]. Our analysis suggests a 6% yield for N as NO$_x$ produced by nitrification associated with the disposal of human and animal waste in central China. We caution that the actual value could be either higher or lower. There is a need for additional observations with a particular emphasis on the fate of nitrogen in animal waste.

[58] A quantity of N of magnitude 7.5 Mt N/yr was applied in the form of chemical fertilizer to agricultural systems in central China in 2001 according to official statistics [NBS, 2002], roughly comparable to the source of N inferred here for human and animal waste. Field studies indicate that the yield for N as NO$_x$ from fertilized soils is significantly higher than that from bare unfertilized soils [Slemr and Seiler, 1984]. The yield reported from various field measurements is generally on the order of 3% [Hutchinson and Brams, 1992; Slemr and Seiler, 1984], under some circumstances as high as 11% [Shepherd et al., 1991]. Field observations in China focus mainly on N$_2$O emissions from fertilized soils and the yield for N as N$_2$O is generally on the order of 1% [Li et al., 2001; Xing and Zhu, 2000; Chen et al., 2002]. Applying a NO/N$_2$O (mole N/ mole N) ratio of 3 would imply a yield of 3% for NO$_x$, consistent with direct observations of NO. A yield of 3% would imply a source of NO$_x$ from chemical fertilizer of 0.23 Tg N/yr, or 0.76 Tg NO$_2$/yr, corresponding to 34% of combustion sources in the Streets et al. [2003] inventory. A lower yield for NO$_x$ from fertilizer application as compared to waste disposal could be attributed to higher levels of O$_2$ in media subject to the former.

[59] The analysis outlined here indicates that emissions of NO$_x$ from waste disposal and fertilizer application in central China could be as large as 2.3 Tg NO$_2$/yr (0.7 Tg N/yr), comparable to emissions reported in the "bottom-up" inventory for combustion. The same methodology applied to south China would imply a source of 0.76 Tg NO$_2$/yr from waste disposal with 0.35 Tg NO$_2$/yr from fertilizer

Table 4. CO and NO$_x$ Emissions by Sector[a]

| Region | Species | A Priori Emissions by Sector (Combustion Only)[b] | | | | | A Priori Total | A Posteriori Total (Uncertainty) | A Posteriori Combustion Sources[c] | Noncombustion NO$_x$[d] |
		Domestic Fuel	Industry	Transport	Power	Biomass				
Central China	CO	12.65	3.95	6.29	0.00	0.14	23.0	41 ($\sim$39.5–42.5)	41	
	NO$_x$	0.13	0.50	0.59	0.98	0.005	2.2	6.3 ($\sim$6.1–6.5)	3.9	2.4
	CO/NO$_x$	165.6	13.0	17.5	0.0	49.3	17.1	10.7 ($\sim$9.8–11.2)	17.2	
South China	CO	8.66	4.35	11.66	0.00	0.3	25.0	47 ($\sim$45–49)	47	
	NO$_x$	0.16	0.75	0.99	0.74	0.009	2.7	3.9 ($\sim$3.7–4.1)	2.8	1.1
	CO/NO$_x$	90.10	9.54	19.29	0.00	56.3	15.5	19.7 ($\sim$18–21.7)	27.5	

[a]A priori emissions by sector are taken from *Streets et al.* [2003], except for biomass-burning emissions, which are from *Duncan et al.* [2003].
[b]Units are Tg CO/yr and Tg NO$_2$/yr for emissions. CO/NO$_x$ emission ratios are expressed in units of mol/mol.
[c]The balance between a posteriori total and noncombustion NO$_x$ sources.
[d]Estimated NO$_x$ emissions from waste disposal and fertilizer (see text).

applications amounting to 40% of the source from combustion. Lower emissions from microbial sources in south as compared to central China reflect differences in human and animal populations and differences in patterns of fertilizer use.

5.3. Combustion Sources of CO and NO$_x$

[60] We consider in this section the uncertainties in CO and NO$_x$ sources associated with combustion processes in order to fully reconcile results from the inversion analysis with the "bottom-up" approach. The inversion analysis provides only composite emissions of CO and NO$_x$ from different geographical regions. To investigate which combustion sectors are most likely to be underestimated in China, we need to examine emissions of CO and NO$_x$ from different sectors as well as ratios of emissions. We assume here that the sector-aggregated CO/NO$_x$ emission ratios in the "bottom-up" approach are correct at least to a first approximation. Given that emission factors for CO and NO$_x$ vary over an order of magnitude for different combustion sources (CO/NO$_x$ ratios vary from about 10 mol/mol for industrial sources to as much as 100 mol/mol for domestic combustion), this approach appears reasonable. The strategy is to identify the sector(s) for which emissions must be adjusted compared to the a priori reference in order to obtain a posteriori CO/NO$_x$ ratios for composite emissions.

[61] Table 4 lists a priori emissions of CO and NO$_x$ for different sectors together with related CO/NO$_x$ emission ratios (mol/mol). *Streets et al.* [2003] adopted emission control standards applicable for power plants in developed countries, assuming accordingly negligible emissions of CO from this sector in China. The table includes a summary of CO and NO$_x$ emissions and ratios for both the a priori and a posteriori inventories with results in the latter case accounting for analysis of the combined TRACE-P and Chinese station data. Results are given for the regions of central and south China that can be constrained independently using the integrated observations and that are defined consistently in the inverse analysis for both CO and NO$_x$ (Figure 3). Sources of NO$_x$ inferred for waste disposal and fertilizer as estimated above (last column in Table 4) are subtracted from a posteriori emissions, with the balance indicated as "a posteriori combustion sources." A posteriori combustion sources of CO are essentially the same as the values discussed earlier since secondary sources of CO contributed by oxidation of methane and biogenic NMVOCs were included from the outset under RW in the inversion analysis.

[62] Combustion sources of CO and NO$_x$ are increased for central China by 75% and 77%, respectively, while the a posteriori CO/NO$_x$ emission ratio (17 mole/mole) remains essentially the same as in the a priori inventory. To maintain the ratio of emissions while realizing an increase in emissions of both CO and NO$_x$, a promising approach would appear to indicate an increase in emissions of both gases from a sector distinguished by a CO/NO$_x$ emission ratio close to the composite ratio of 17. Allowing for possible errors associated with emission ratios in the "bottom-up" approach, candidates to resolve the discrepancy in emissions would appear to favor the transportation (with CO/NO$_x$ = 17.5) and the industrial (with CO/NO$_x$ = 12.8) sectors. Combustion of fossil fuel (i.e., coal and oil) is responsible for the dominant source of CO and NO$_x$ from these two sectors. If all of the required increase was attributed solely to these two sectors, we would need to invoke an increase in associated NO$_x$ and CO emissions by at least a factor of 2. We discuss below the extent to which uncertainties in activity rates (i.e., coal and oil consumption) and emission factors could account for the required increase.

[63] Some studies suggest that China's petroleum consumption may be larger than reported, reflecting in this case failure to recognize oil imported illegally by smuggling into Southeast China in the later half of the 1990s [*U.S. Embassy in Beijing*, 2001] (available at http://www.usembassy-china. org.cn/sandt/energy_stats_web.htm). Official data indicate that gasoline consumption rose by just 10% from 1996 to 2000, while the number of registered civilian vehicles increased by 30% and public transport passenger miles increased by 24% [*NBS*, 2001]. It has been suggested further that rural vehicles not included in the official statistics may also have contributed to the underestimate in related emissions (D. Streets, personal communication, 2004). It is noteworthy that any explanation that involves raising the amount of fuel burned to accommodate the inverse modeling results for NO$_x$ and CO will also probably increase emissions of other species such as SO$_2$, and needs further investigation.

[64] If the underestimate of emissions is attributed to an underestimate of emission factors, we would need to invoke an increase in emission factors for CO and NO$_x$ by over 70%. We could account for the data in Table 4 if emission factors for NO$_x$ and CO associated with coal combustion in the industrial sector were increased to 9 (kg NO$_2$/t coal) and 63 (kg CO/t coal), respectively. For the transportation sector, we would need to increase emission factors for

NO$_x$ to 35 kg NO$_2$/t on average for gasoline-powered vehicles, 45 kg NO$_2$/t for diesel vehicles. Adjustments in emission factors of this magnitude would be within the range of values quoted by *Streets et al.* [2003]. For comparison, the highest emission factor for NO$_x$ from coal-fired boilers reported by the *U.S. Environmental Protection Agency* (*USEPA*) [1972, 1985, 1995] (the latter is available at http://www.epa.gov/ttn/chief/ap42/index.html) is 17 kg NO$_2$/t coal. The U.S. EPA suggested emission factors of 28 kg NO$_2$/t for gasoline vehicles and 49 kg NO$_2$/t for diesel vehicles in the early 1970s [*USEPA*, 1972]. A large increase in emission factors for CO is likely for China if the combustion efficiency is underestimated in the industry sector or the transportation sector. The above analysis suggests that increases in emission factor would be required to account for a doubling of emissions of CO and NO$_x$ from the combustion of coal and oil in central China.

[65] For south China, our analysis suggests that combustion sources of CO and NO$_x$ should be increased by 88% and 4%, respectively. Emissions from domestic fuel and biomass burning would need to be increased selectively to adjust the composite CO/NO$_x$ emission ratio from 15.5 (a priori) to 27.5 (a posteriori). Since these two sectors contribute less than 5% of total NO$_x$ emissions in this region, it would be possible to obtain a large increase in CO emissions but only a small increase in NO$_x$ emissions by a selective increase in activities for these sectors. Accommodating the constraints implied by the inversion analysis would require an increase in emissions of CO emissions by as much as a factor of 4.

[66] A reanalysis of CO emissions for the TRACE-P mission period is currently underway. An interesting early product of this analysis involves an upward revision of "bottom-up" emissions for CO. The new results are generally consistent with the conclusions independently reached here on the basis of our study of the combined aircraft/ station database. The modified "bottom-up" inventory increases CO emissions from the industry sector in China by over 70%, mostly because of a reassessment of small industrial coal-burning sources (D. G. Streets et al., Revisiting China's CO emissions after TRACE-P: Synthesis of inventories, atmospheric modeling, and observations, manuscript in preparation, 2004). The adjustments differ from province by province, but the largest increases occur for provinces in the central region of China (Q. Zhang, Tsinghua University, personal communication, 2004).

6. Analysis of Surface Measurements Using A Posteriori Emissions

[67] This section presents a detailed analysis of the surface observations for Hong Kong and Lin An using the forward model with a posteriori emissions. Specific objectives are to explore factors other than emissions that impact concentrations of pollutants at the two stations and to assess the ability of the forward model to simulate "near source" situations over China. Most of the attention is directed here to CO.

[68] Variations in CO at the two stations are driven mainly by transport rather than by chemistry reflecting the relatively long lifetime for CO over the time interval (February to April) selected for the present study. The nested model captures observed changes in CO at the two stations satisfactorily, with correlation coefficient of about 0.8 for Hong Kong and 0.7 for Lin An. This suggests that the model is capable of providing an adequate account of the meteorological factors that are primarily responsible for the temporal variations in CO observed over east China during late winter and early spring. An important synoptic feature of the weather over China during this time involves the southeastward moving cold front [*Lau and Li*, 1984]. Concentrations of CO and NO$_y$ at the two stations respond to this phenomenon typically on a timescale of 5–7 days. It has been established in several TRACE-P studies that lifting ahead of the cold front represents one of the major pathways for export of CO emitted in south China to the free troposphere [*Liu et al.*, 2003; *Y. Wang et al.*, 2004]. Impacts of the cold front on surface CO concentrations may be illustrated by associating changes in CO with changes in surface temperature (Figures 18 and 19), since rapid drops in temperature provide a useful proxy for the passage of cold fronts [*Liu et al.*, 2003].

[69] The temperature data for Hong Kong and Lin An, depicted in Figures 18b and 19b, respectively, were taken from the model input (black lines) and from radiosonde observations (red lines) reported by the National Climatic Data Center (NCDC) and the Forecast Systems Laboratory (FSL) of NOAA (NCDC and FSL Radiosonde Database, 2004, available from http://raob.fsl.noaa.gov/). Radiosonde measurements are not available for Lin An. In this case, we used observations from Hang Zhou (30.23°N, 120.17°E), a city 53 km east of Lin An but in the same model grid as Lin An. Two radiosonde measurements are carried out per day: at 0000 UTC (7 A.M. local time) and 1200 UTC (7 P.M. local time) for Hong Kong and at 1100 UTC (6 P.M. local time) and 2300 UTC (6 A.M. local time) for Hang Zhou. Since we are interested primarily in day-to-day variations in meteorology, we choose to use the afternoon meteorological data to represent the daily situation, sampling model outputs for CO and NO$_y$ for the specific times of the corresponding measurements. The comparison between model and observed temperatures indicates that the model successfully simulates observed day-to-day changes in temperature both for Hong Kong (Figure 18b) and for Lin An (Figure 19b). The correlation coefficient between model and observations is 0.92 at Hong Kong and 0.90 at Lin An.

[70] The association of changes in CO with changes in surface temperature at Hong Kong is illustrated in Figure 18 with CO concentrations presented in Figure 18a, with surface temperatures in Figure 18b. Figure 18a compares CO observations (red line) with model CO results obtained using a posteriori emissions (black line). The model successfully predicts almost all the major peaks in CO concentrations. Almost all of the peaks in CO are associated with drops in surface temperature, reflecting presumably passages of the cold front. The "cold events," indicated by blue dashed lines in Figures 18a and 18b, occur more frequently in March than in April. Figure 20 presents monthly mean wind patterns for the atmosphere below 1 km (black arrows) and sea level pressures (color coding) for March (Figure 20a) and April 2001 (Figure 20b). The data shown are taken from the GEOS-3 assimilated meteorology. The northwesterly winter monsoon dominates conditions over most of China in March while it begins to
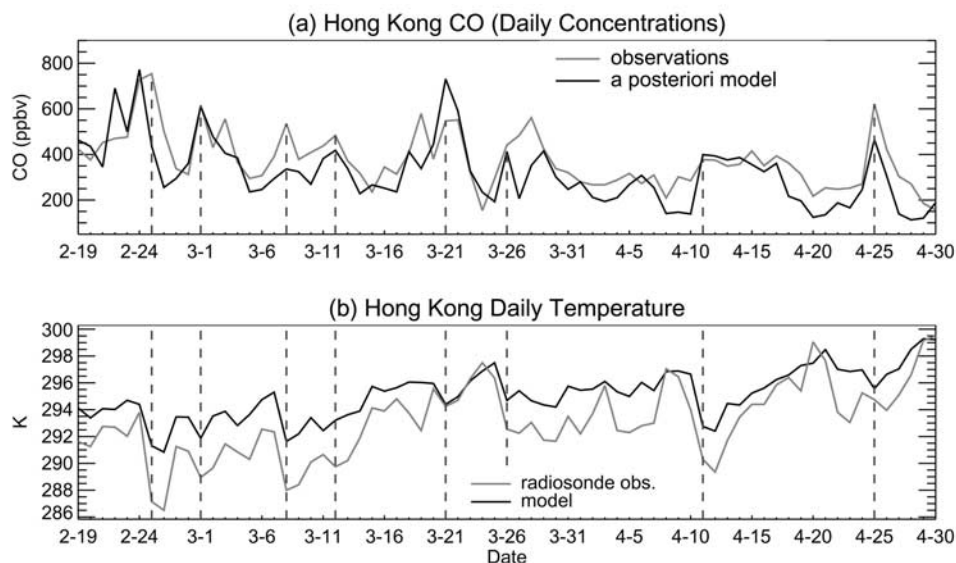
Figure 18. (a) Daily CO concentrations and (b) daily average surface temperatures at Hong Kong. Observations are shown in red, and model predictions are shown in black. The "cold events" are indicated by blue dashed lines. See color version of this figure at back of this issue.

abate in April. The cold front is located typically at the leading edge of strong cold air outbreaks following the same direction as the prevailing monsoonal winds, from northwest to southeast. Southeastward advection of cold air behind the cold front brings polluted air from the north and east where emissions are high (Figure 1), resulting in an increase in CO at Hong Kong. Our tagged tracer simulation suggests that over 80% of surface CO at Hong Kong during the study period originates from sources outside of the central-south China region where Hong Kong is located. The success of the model in simulating the association between CO peaks and temperature drops demonstrates the ability of the model to account for the timing and spatial extent of cold front passages.

[71] Results for Lin An are presented in Figure 19. The model using a posteriori emissions is successful in simulating most of the CO peaks observed before 1 April but fails to reproduce peaks observed after 1 April. The peaks in CO prior to 1 April, captured by the model, are generally associated with drops in temperature, while the peaks missed by the model after 1 April are associated often with increases in surface temperature. "Cold events" are indicated by blue dashed lines with "warm events" after 1 April by orange dashed lines in Figure 19. Similar to Hong Kong, the "cold events" at Lin An are generally associated with passages of the cold front carrying polluted air from the northwest and are simulated well by the model. It is interesting to notice that the "cold events" at Lin An often precede those at Hong Kong, illustrating the southward passage of the cold fronts. The mechanism of the "warm events" has not been addressed in literature, according to our knowledge. That they occur only in April suggests that they may be related to the transition in meteorological conditions that takes place at this time. Wind patterns below 1 km and sea level pressure from the GEOS-3 data for April 2001, reproduced in Figure 20b, indicate on a monthly mean basis the presence of an anticyclone over the Yellow

Sea. Lin An is located at the southern edge of the anticyclone, downwind of the Shanghai metropolitan region and the YRD industrial zone to the northeast. As we shall show, the anticyclone, depicted in the monthly mean map of Figure 20b, reflects an average effect of intruding high-pressure systems from the ocean to the east, compensated by occasional southward movement of low-pressure systems to the north. Day-to-day variations in the location and strength of the anticyclone determines whether Lin An receives polluted air from the northeast (Shanghai and YRD), aged polluted air from the southwest (inland China), or relatively clean air from the southeast (rural and ocean).

[72] A summary of wind directions at 925 mbar obtained from radiosonde (red lines) and model (black lines) data for the Lin An site is presented in Figure 19c. Model wind directions for the "cold events" (indicated by blue dashed lines), always from the northwest, are in good agreement with observation. In contrast, wind directions in the model for the four "warm events" (i.e., 2, 6, 15, and 29 April) differ significantly from observation. Inspection of model and observed surface pressures suggests that the model does a satisfactory job in simulating the pressure changes observed at Lin An (Figure 19d). A mismatch in wind directions appears to be primarily responsible for the failure of the model to capture the high-CO peaks observed during the "warm events." Analysis of pressure data and observed afternoon concentrations of O$_3$ at Lin An (not shown) indicates that the 6 April and 15 April warm events were associated with high pressures and high concentrations of O$_3$ (60–70 ppb), while the 2 April and 29 April events were distinguished by low pressure and low O$_3$ (30 ppb).

[73] Radiosonde measurements indicate that the wind was directed from the northeast at Lin An on 6 April under the influence of a high-pressure system (Figures 19c and 19d), suggesting that Lin An was positioned to the southeast of an anticyclone and thus directly downwind of Shanghai and the YRD. Besides CO (>800 ppb), high concentrations of
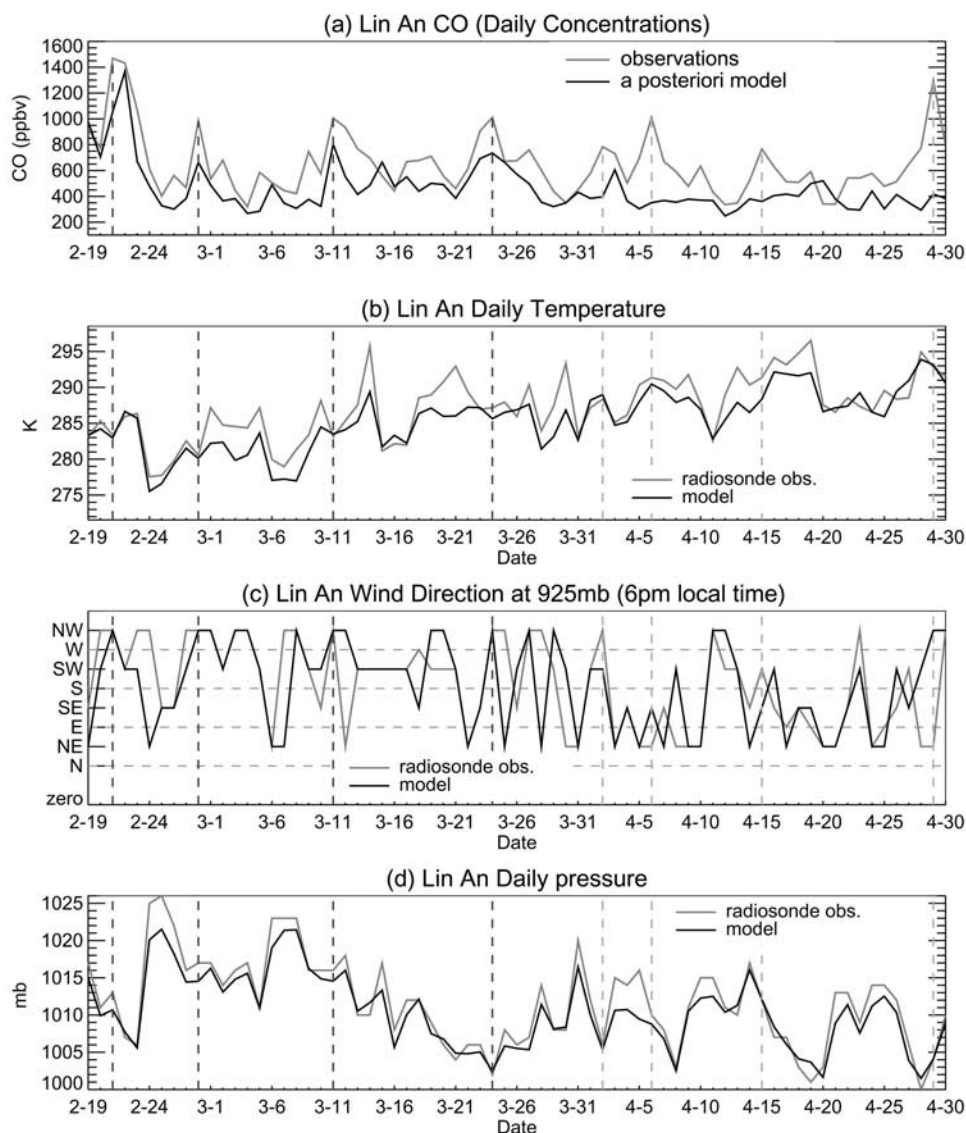
Figure 19. (a) Daily CO concentrations, (b) daily average surface temperatures, (c) wind directions at 925 mbar, and (d) surface pressure at Lin An. Observations are shown in red, and model predictions are shown in black. The ''cold events'' are indicated by blue dashed lines, and ''warm events'' are indicated by orange dashed lines. See color version of this figure at back of this issue.

SO$_2$ (>20 ppb), NO (>2 ppb) and NO$_y$ (~15 ppb) were also observed at Lin An on 6 April. The increase in surface temperature was due to intrusion of warm marine air from the east. Warm temperatures, weak winds and stable conditions associated with the high-pressure system favor production of high levels of O$_3$. In the model, however, the anticyclone was located to the northeast of Lin An (rather than to north or northwest as indicated by the observations) and that the wind originated generally from the southeast (Figure 21a). The influence of plumes from Shanghai and the YRD was limited in the model to one grid north of Lin An while Lin An received relatively clean air from the southeast. For the 29 April event, radiosonde observations indicate that the wind was directed from the northeast at Lin An under the influence of a low-pressure system (Figures 19c and 19d), implying that Lin An was located to the northwest of the low-pressure system and thus

directly downwind of Shanghai and the YRD. Again, surface temperature increases occurred as a consequence of the intrusion of warm marine air from the east. Ozone production is not favorable in the low-pressure system. The GEOS-3 data adopted in the model imply that Lin An was located to the southwest of the low-pressure receiving air from the northwest rather than the northeast as indicated by the observations (Figure 21b). The influence of YRD plumes in the model was confined to grids northeast of Lin An and CO levels predicted for Lin An were comparatively low.

[74] Analyses of the April ''warm events'' indicate deficiencies in the meteorological data (i.e., the GEOS-3 data with resolution 1° × 1°) used to drive the chemical transport model in terms of the ability of the model to simulate changes associated with relatively small-scale weather systems (smaller than 1° × 1° resolution). While larger-scale
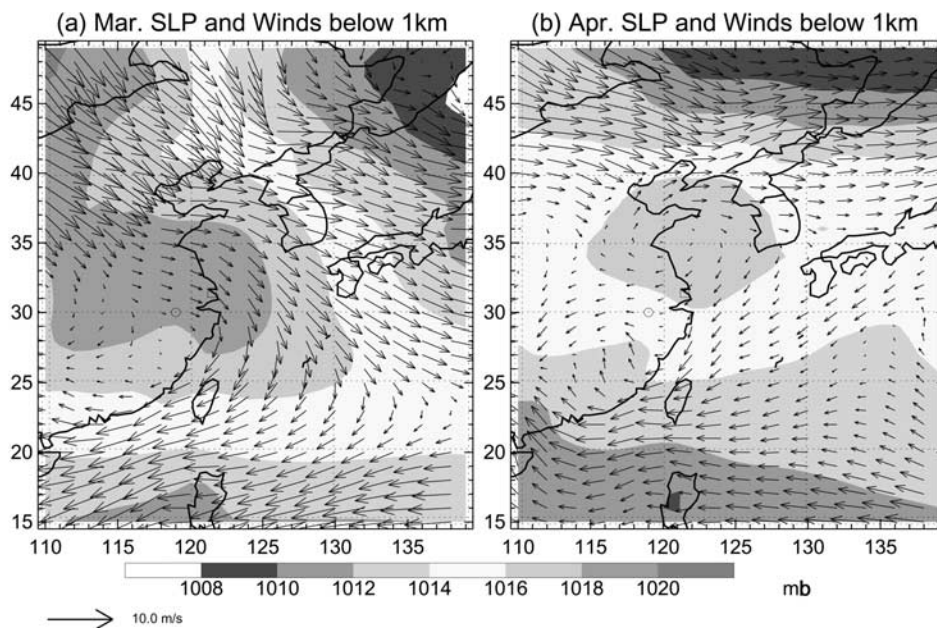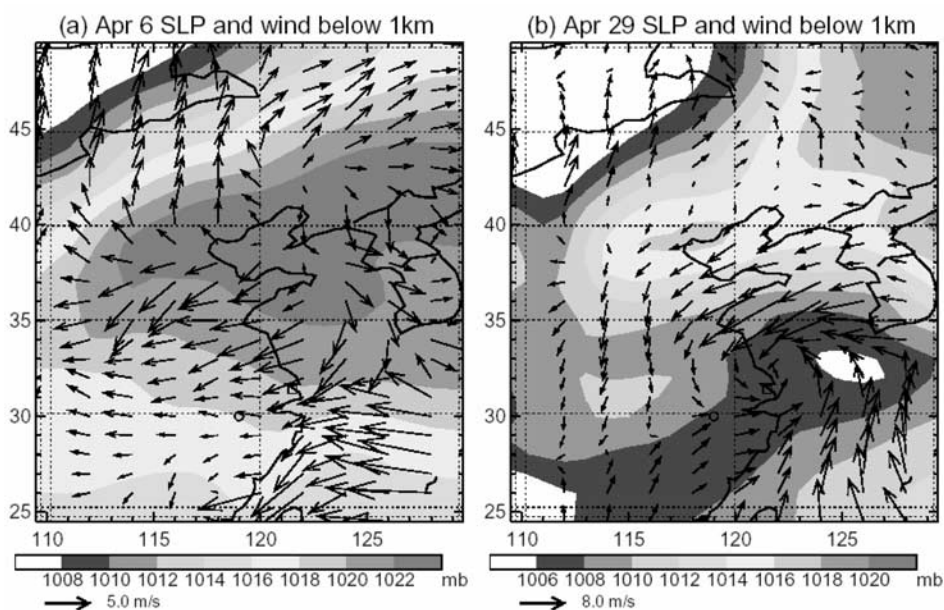
Figure 20. Sea level pressure (SLP; color coding) and wind patterns below 1 km (black arrows) for (a) March and (b) April 2001. The data shown are from the GEOS-3 assimilated meteorology. The locations of Lin An (119°E, 30°N) and Shanghai (121.5°E, 31.4°N) are indicated by an open circle and an open square, respectively. See color version of this figure at back of this issue.

features such as pressure and temperature are captured satisfactorily by the model, a slight mismatch in simulation of the exact position of high- and low-pressure systems with the GEOS-3 data was found to result in occasional errors in wind directions for Lin An with a consequent underestimate of concentrations for CO. The problem is attributed to the sensitivity of the source-receptor relationship linking the YRD (including Shanghai) and Lin An. The mismatch in model meteorology in April, however, should not impact conclusions reached concerning emissions. Errors implicit in the forward model as employed in the inversion analysis are greater for April than for March and February at Lin An

Figure 21. Sea level pressure (color coding) and wind patterns below 1 km (black arrows) for (a) 6 April and (b) 29 April 2001. The data shown are from the GEOS-3 assimilated meteorology. The locations of Lin An (119°E, 30°N) and Shanghai (121.5°E, 31.4°N) are indicated by an open circle and an open square, respectively. Note that the two figures have a different color scale for SLP and arrow length for wind speed. See color version of this figure at back of this issue.

(section 3.3). An inversion analysis excluding the April data at Lin An found no significant differences in resulting a posteriori emissions.

7. Concluding Remarks

[75] Previous modeling studies offer compelling evidence that Chinese anthropogenic emissions of CO are underestimated in the bottom-up analysis published by *Streets et al.* [2003]. Unexplored is the implication of the underestimate of CO emissions for other combustion-related species such as NO$_x$. This study used measurements of NO$_y$ as a surrogate to diagnose emissions of NO$_x$ since emissions of NO$_x$ provide the only significant source of NO$_y$. Observations of CO and NO$_y$ from the TRACE-P aircraft mission over the NW Pacific, and two Chinese ground stations, Hong Kong and Lin An, during the spring of 2001 were used in conjunction with an optimal estimation inverse model to develop independent constraints for Asian emissions of CO and NO$_x$.

[76] A priori emissions and associated uncertainties were taken from *Streets et al.* [2003]. We used the $1° \times 1°$ nested-grid GEOS-CHEM model in the forward mode [*Y. Wang et al.*, 2004] to examine the consistency of the Streets et al. inventory with results obtained from the TRACE-P aircraft mission and the surface stations. The nested-grid model satisfactorily accounted for the observed variations of CO and NO$_y$ but significantly underestimated absolute values for the concentrations of both species. The shortfall for the observations at Lin An was up to a factor of 2 for CO and a factor of 3 for NO$_y$. We argued that there are no systematic biases in the forward model in terms of NO$_y$ chemistry or relative deposition rates. This allowed for the assumption of a linear relationship between NO$_x$ sources and concentrations of NO$_y$. A simple test of this linearity was implemented by comparing the sum of tagged NO$_y$ tracer concentrations scaled by emission adjustments with NO$_y$ concentrations obtained from the model using adjusted NO$_x$ emissions. We verified that results obtained by summing scaled concentrations were identical to those obtained with the model using scaled emissions.

[77] The TRACE-P aircraft and surface observations differ in their ability to independently constrain sources. The aircraft data impose constraints on background contributions as well as regional sources, but have limited ability to constrain subregional sources for China, especially for relatively short-lived species such as NO$_y$. The observations at the two surface stations have the advantage of high temporal resolution at fixed locations with high sensitivity to nearby emissions, allowing thus for constraints on subregional sources in China. The integrated observational system (i.e., TRACE-P and surface observations) was found to provide independent constraints on emissions from specific subregions of China: for north, central, and south China in the case of CO and for central and south China in the case of NO$_x$.

[78] The inversion analysis required increases of 43% and 47% for Chinese emissions of CO and NO$_x$, respectively, distributed heterogeneously with the largest adjustments for central China. A posteriori estimates of emissions from biomass burning in Southeast Asia are much lower than a priori values, consistent with conclusions reached in other TRACE-P studies. Inversion results for NO$_x$ emissions are consistent with CO emissions in terms of the sense of the adjustments. Different sensitivity studies suggest that a posteriori emissions are robust and relatively insensitive to assumptions concerning deposition rates of NO$_y$. A posteriori emissions of CO and NO$_x$ from central China are increased by 75% and 189%, respectively, relative to a priori values. Increases for south China amount to 87% for CO, 47% for NO$_x$. The large increases in emissions inferred for central and south China are driven mainly by the need to correct for the underestimate of the model using a priori emissions of the surface measurements at Lin An (central China) and Hong Kong (south China), reinforced by a similar underestimate of TRACE-P observations for the boundary layer between 25°N and 35°N [*Y. Wang et al.*, 2004]. Inclusion of the surface station data in the inversion analysis allowed for a significant improvement in estimates of emissions from central and south China.

[79] The increase in NO$_x$ emissions inferred for central China is too large to be accommodated by any reasonable adjustment in sources contributed by combustion of either fossil or biofuel. We proposed that the missing source of NO$_x$ may be associated significantly with microbially mediated decomposition of human and animal wastes under oxygen stressed conditions and with intensive use of chemical fertilizer. Nitrification represents an important source of both NO and N$_2$O and it is well established that yields of both species are enhanced at conditions of low oxygen. The potential source of NO from fertilizer and the human-animal food chain was estimated using data for fertilizer use and for human and animal populations combined with plausible estimates for potential yields of NO. We concluded that microbial activities could account for a source of NO in China comparable to that associated with combustion.

[80] Analyses of ratios of CO to NO$_x$ inferred from the inverse study were used to further refine estimates for combustion related sources of these species. We concluded that emissions from the industrial and transportation sectors were most likely underrepresented in the "bottom-up" inventory for central China, while emissions from the domestic sector may be understated for south China. A combination of increases in activity rates and emission factors were discussed which could help reconcile conclusions reached in the inversion analysis with results from the "bottom-up" approach.

[81] Finally, a detailed analysis of the surface observations using a posteriori emissions established the association of variations in CO with changes in meteorological conditions, notably the passage of cold fronts in March and the small-scale high- and low-pressure systems that develop over central China in April. While larger-scale features such as pressure and temperature are captured satisfactorily by the model, a slight mismatch in the simulation of the exact position of high- and low-pressure systems by the GEOS-3 data was found to result in occasional errors in wind directions for Lin An with a consequent underestimate of concentrations for CO. The problem was attributed to the sensitivity of the source-receptor relationship linking the YRD (including Shanghai) and Lin An. The mismatch in model meteorology in April had no effect, however, on conclusions reached concerning emissions.

References

Allen, D. J., R. B. Rood, A. M. Thompson, and R. D. Hudson (1996), Three dimensional radon 222 calculations using assimilated meteorological data and a convective mixing algorithm, *J. Geophys. Res.*, *101*, 6871–6881.

Arellano, A. F., Jr., P. S. Kasibhatla, L. Giglio, G. R. van der Werf, and J. T. Randerson (2004), Top-down estimates of global CO sources using MOPITT measurements, *Geophys. Res. Lett.*, *31*, L01104, doi:10.1029/2003GL018609.

Bey, I., D. J. Jacob, R. M. Yantosca, J. A. Logan, B. Field, A. M. Fiore, Q. Li, H. Liu, L. J. Mickley, and M. Schultz (2001), Global modeling of tropospheric chemistry with assimilated meteorology: Model description and evaluation, *J. Geophys. Res.*, *106*, 23,073–23,096.

Carmichael, G. R., et al. (2003), Evaluating regional emission estimates using the TRACE-P observations, *J. Geophys. Res.*, *108*(D21), 8810, doi:10.1029/2002JD003116.

Chatfield, C. (1995), *The Analysis of Time Series: An Introduction*, p. 20, Chapman and Hall, New York.

Chen, X., M. L. Cabrera, L. Zhang, J. Wu, Y. Shi, W. T. Yu, and S. M. Shen (2002), Nitrous oxide emission from upland crops and crop-soil systems in northeastern China, *Nutrient Cycling Agroecosyst.*, *62*, 241–247.

Czepiel, P., E. Douglas, R. Harriss, and P. Crill (1996), Measurements of N$_2$O from composted organic wastes, *Environ. Sci. Technol.*, *30*, 2519–2525.

DeMore, W. B., S. P. Sander, D. M. Golden, R. F. Hampson, M. J. Kurylo, C. J. Howard, A. R. Ravishankara, C. E. Kolb, and M. J. Molina (1997), Chemical kinetics and photochemical data for use in stratospheric modeling, *JPL Publ.*, *97-4*.

Duncan, B. N., R. V. Martin, A. C. Staudt, R. Yevich, and J. A. Logan (2003), Interannual and seasonal variability of biomass burning emissions constrained by satellite observations, *J. Geophys. Res.*, *108*(D2), 4100, doi:10.1029/2002JD002378.

Fiore, A. M., D. J. Jacob, I. Bey, R. M. Yantosca, B. D. Field, A. C. Fusco, and J. G. Wilkinson (2002), Background ozone over the United States in summer: Origin, trend, and contribution to pollution episodes, *J. Geophys. Res.*, *107*(D15), 4275, doi:10.1029/2001JD000982.

Heald, C. L., D. J. Jacob, P. I. Palmer, M. J. Evans, G. W. Sachse, H. B. Singh, and D. R. Blake (2003), Biomass burning emission inventory with daily resolution: Application to aircraft observations of Asian outflow, *J. Geophys. Res.*, *108*(D4), 8368, doi:10.1029/2002JD002732.

Heald, C. L., D. J. Jacob, D. B. A. Jones, P. I. Palmoer, J. A. Logan, D. G. Streets, G. W. Sachse, J. C. Gille, R. N. Hoffman, and T. Nehrkorn (2004), Comparative inverse analysis of satellite (MOPITT) and aircraft (TRACE-P) observations to estimate Asian sources of carbon monoxide, *J. Geophys. Res*, doi:10.1029/2004JD005185, in press.

Horowitz, L. W., J. Liang, G. M. Gardner, and D. J. Jacob (1998), Export of reactive nitrogen from North America during summertime: Sensitivity to hydrocarbon chemistry, *J. Geophys. Res.*, *103*, 13,451–13,476.

Hutchinson, G. L., and E. A. Brams (1992), NO versus N$_2$O emissions from an NH$_4^+$-amended Bermuda grass pasture, *J. Geophys. Res.*, *97*, 9889–9896.

Intergovernmental Panel on Climate Change (IPCC) (1996), *Greenhouse Inventory Reference Manual*, chap. 4, Geneva.

Jacob, D. J. (2000), Heterogeneous chemistry and tropospheric ozone, *Atmos. Environ.*, *34*, 2131–2159.

Jacob, D. J., J. H. Crawford, M. M. Kleb, V. S. Connors, R. J. Bendura, J. L. Raper, G. W. Sachse, J. C. Gille, L. Emmons, and C. L. Heald (2003), The Transport and Chemical Evolution over the Pacific (TRACE-P) aircraft mission: Design, execution, and first results, *J. Geophys. Res.*, *108*(D20), 9000, doi:10.1029/2002JD003276.

Kasibhatla, P., A. Arellano, J. A. Logan, P. I. Palmer, and P. Novelli (2002), Top-down estimate of a large source of atmospheric carbon monoxide associated with fuel combustion in Asia, *Geophys. Res. Lett.*, *29*(19), 1900, doi:10.1029/2002GL015581.

Lau, K. M., and M. T. Li (1984), The monsoon of east Asia and its global associations, *Bull. Am. Meteorol. Soc.*, *65*(2), 114–125.

Lee, D. S., et al. (1997), Estimates of global NO$_x$ emissions and their uncertainties, *Atmos. Environ.*, *31*(12), 1735–1749.

Li, C., et al. (2001), Comparing a process-based agro-ecosystem model to the IPCC methodology for developing a national inventory of N$_2$O emissions from arable lands in China, *Nutrient Cycling Agroecosyst.*, *60*, 159–175.

Lipschultz, F., O. C. Zafiriou, S. C. Wofsy, M. B. McElroy, F. W. Valois, and S. W. Watson (1981), Production of NO and N$_2$O by soil nitrifying bacteria: A source of atmospheric nitrogen oxides, *Nature*, *294*, 641–643.

Liu, H., D. J. Jacob, I. Bey, and R. M. Yantosca (2001), Constrains from ^{210}Pb and ^{7}Be on wet deposition and transport in a global three-dimensional chemical tracer model driven by assimilated meteorological fields, *J. Geophys. Res.*, *106*, 12,109–12,128.

Liu, H. Y., D. J. Jacob, I. Bey, R. M. Yantosca, B. N. Duncan, and G. W. Sachse (2003), Transport pathways for Asian combustion outflow over the Pacific: Interannual and seasonal variations, *J. Geophys. Res.*, *108*(D20), 8786, doi:10.1029/2002JD003102.

Logan, J. A. (1983), Nitrogen oxides in the troposphere: Global and regional budgets, *J. Geophys. Res.*, *88*, 10,785–10,807.

Martin, R. V., D. J. Jacob, R. M. Yantosca, M. Chin, and P. Ginoux (2003), Global and regional decreases in tropospheric oxidants from photochemical effects of aerosols, *J. Geophys. Res.*, *108*(D3), 4097, doi:10.1029/2002JD002622.

McElroy, M. B. (1980), Sources and sinks for nitrous oxide, *Rep. FAA-EE-80-20*, U.S. Dep. of Transp., Washington, D. C.

McElroy, M. B., et al. (1978), Production and release of N$_2$O from Potomac estuary, *Limnol. Oceanogr.*, *23*(6), 1168–1182.

Munger, J. W., S.-M. Fan, P. S. Bakwin, M. L. Goulden, A. H. Goldstein, A. S. Colman, and S. C. Wofsy (1998), Regional budgets for nitrogen oxides from continental sources: Variations of rates for oxidation and deposition with season and distance from source regions, *J. Geophys. Res.*, *103*, 8355–8368.

National Bureau of Statistics of China (NBS) (2001), *China Transportation Yearbook 2000*, China Stat. Press, Beijing.

National Bureau of Statistics of China (NBS) (2002), *China Statistical Yearbook 2001*, China Stat. Press, Beijing.

National Research Council Committee on Nitrate Accumulation (1972), *Accumulation of Nitrate*, Natl. Acad. of Sci., Washington, D. C.

Palmer, P. I., D. J. Jacob, D. B. A. Jones, C. L. Heald, R. M. Yantosca, J. A. Logan, G. W. Sachse, and D. G. Streets (2003), Inverting for emissions of carbon monoxide from Asia using aircraft observations over the western Pacific, *J. Geophys. Res.*, *108*(D21), 8825, doi:10.1029/2002JD003176.

Parrish, D. D., M. Trainer, M. P. Buhr, B. A. Watkins, and F. C. Fehsenfeld (1991), Carbon monoxide concentrations and their relation to concentrations of total reactive oxidized nitrogen at two rural U.S. sites, *J. Geophys. Res.*, *96*, 9309–9320.

Roberts, J. M. (1995), Reactive odd-nitrogen (NO$_y$) in the atmosphere, in *Composition, Chemistry, and Climate for the Atmosphere*, edited by H. B. Singh, pp. 176–215, Van Nostrand Reinhold, New York.

Rodgers, C. D. (2000), *Inverse Methods for Atmospheric Sounding: Theory and Practice*, World Sci., River Edge, N. J.

Russo, R., et al. (2003), Chemical composition of Asian continental outflow over the western Pacific: Results from Transport and Chemical Evolution over the Pacific (TRACE-P), *J. Geophys. Res.*, *108*(D20), 8804, doi:10.1029/2002JD003184.

Seinfeld, J. H., and S. N. Pandis (1998), *Atmospheric Chemistry and Physics: From Air Pollution to Climate Change*, p. 71, John Wiley, Hoboken, N. J.

Shepherd, M. F., S. Barzetti, and D. R. Hastie (1991), The production of atmospheric NO$_x$ and N$_2$O from a fertilized agricultural soil, *Atmos. Environ., Part A*, *25*, 1961–1969.

Sinton, J. E., and D. G. Fridley (2000), What goes up: Recent trends in China's energy consumption, *Energy Policy*, *28*, 671–687.

Slemr, F., and W. Seiler (1984), Field measurements of NO and NO$_2$ emissions from fertilized and unfertilized soils, *J. Atmos. Chem.*, *2*, 1–24.

Streets, D. G., et al. (2003), An inventory of gaseous and primary aerosol emissions in Asia in the year 2000, *J. Geophys. Res.*, *108*(D21), 8809, doi:10.1029/2002JD003093.

Suntharalingam, P., D. J. Jacob, P. I. Palmer, J. A. Logan, R. M. Yantosca, Y. Xiao, M. J. Evans, D. G. Streets, S. L. Vay, and G. W. Sachse (2004), Improved quantification of Chinese carbon fluxes using CO$_2$/CO correlations in Asian outflow, *J. Geophys. Res.*, *109*, D18S18, doi:10.1029/2003JD004362.

Talbot, R., et al. (2003), Reactive nitrogen in Asian continental outflow over the western Pacific: Results from the NASA Transport and Chemical Evolution over the Pacific (TRACE-P) airborne mission, *J. Geophys. Res.*, *108*(D20), 8803, doi:10.1029/2002JD003129.

U.S. Embassy in Beijing (2001), The controversy over China's reported falling energy use, Beijing, Aug.

U.S. Environmental Protection Agency (USEPA) (1972), Compilation of air pollutant emission factors, *Publ. AP-42,* Off. of Air Programs, Research Triangle Park, N. C.

U.S. Environmental Protection Agency (USEPA) (1985), Compilation of air pollutant emission factors: Third edition, update package, *Publ. AP-42*, Research Triangle Park, N. C.

U.S. Environmental Protection Agency (USEPA) (1995), Compilation of air pollutant emission factors: Fifth edition, vol. 1, Stationary point and area sources, *Publ. AP-42*, Research Triangle Park, N. C.

Wang, T., T. F. Cheung, Y. S. Li, X. M. Yu, and D. R. Blake (2002), Emission characteristics of CO, NO$_x$, SO$_2$ and indications of biomass burning observed at a rural site in eastern China, *J. Geophys. Res.*, *107*(D12), 4157, doi:10.1029/2001JD000724.

Wang, T., A. J. Ding, D. R. Blake, W. Zahorowski, C. N. Poon, and Y. S. Li (2003), Chemical characterization of the boundary layer outflow of air pollution to Hong Kong during February–April 2001, *J. Geophys. Res.*, *108*(D20), 8787, doi:10.1029/2002JD003272.

Wang, T., et al. (2004), Relationships of trace gases and aerosols and the emission characteristics at Lin'an, a rural site in eastern China during spring 2001, *J. Geophys. Res.*, *109*, D19S05, doi:10.1029/2003JD004119.

Wang, Y., D. J. Jacob, and J. A. Logan (1998), Global simulation of tropospheric O$_3$-NO$_x$-hydrocarbon chemistry: 1. Model formulation, *J. Geophys. Res.*, *103*, 10,713–10,725.

Wang, Y. X., M. B. McElroy, D. J. Jacob, and R. M. Yantosca (2004), A nested grid formulation for chemical transport over Asia: Applications to CO, *J. Geophys. Res.*, *109*, D22307, doi:10.1029/2004JD005237.

Wesely, M. L. (1989), Parameterization of surface resistance to gaseous dry deposition in regional-scale numerical models, *Atmos. Environ.*, *23*, 1293–1304.

Wild, O., J. K. Sundet, M. J. Prather, I. S. A. Isaksen, H. Akimoto, E. V. Browell, and S. J. Oltmans (2003), Chemical transport model ozone simulations for spring 2001 over the western Pacific: Comparisons with TRACE-P lidar, ozonesondes, and Total Ozone Mapping Spectrometer columns, *J. Geophys. Res.*, *108*(D21), 8826, doi:10.1029/2002JD003283.

Xing, G. X., and Z. L. Zhu (2000), An assessment of N loss from agricultural lands to the environment in China, *Nutrient Cycling Agroecosyst.*, *57*, 67–73.

Yevich, R., and J. A. Logan (2003), An assesment of biofuel use and burning of agricultural waste in the developing world, *Global Biogeochem. Cycles*, *17*(4), 1095, doi:10.1029/2002GB001952.

Yienger, J. J., and H. Levy (1995), Empirical model of global soil-biogenic NO$_x$ emissions, *J. Geophys. Res.*, *100*, 1447–1464.

Zhang, M., et al. (2003), Large-scale structure of trace gas and aerosol distributions over the western Pacific Ocean during the Transport and Chemical Evolution over the Pacific (TRACE-P) experiment, *J. Geophys. Res.*, *108*(D21), 8820, doi:10.1029/2002JD002946.

———————————

M. B. McElroy, P. I. Palmer, and Y. X. Wang, Department of Earth and Planetary Science, Harvard University, 29 Oxford Street, Pierce Hall, Room 107F, Cambridge, MA 02138, USA. (wang3@fas.harvard.edu)

T. Wang, Department of Civil and Structural Engineering, Hong Kong Polytechnic University, Hung Hom, Kowloon, Hong Kong, China.
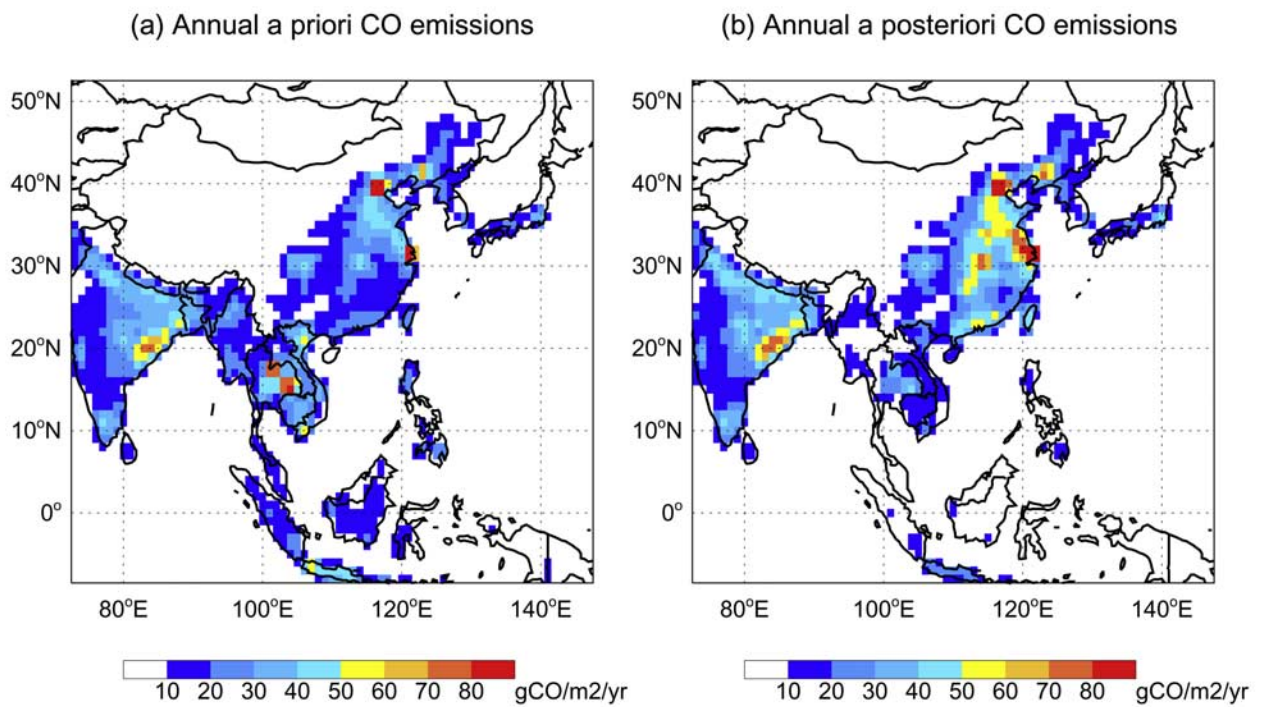
Figure 1. (a) A priori and (b) a posteriori annual emissions of CO for Asia. A posteriori emissions are from the inverse analysis in which both TRACE-P and surface data are employed.
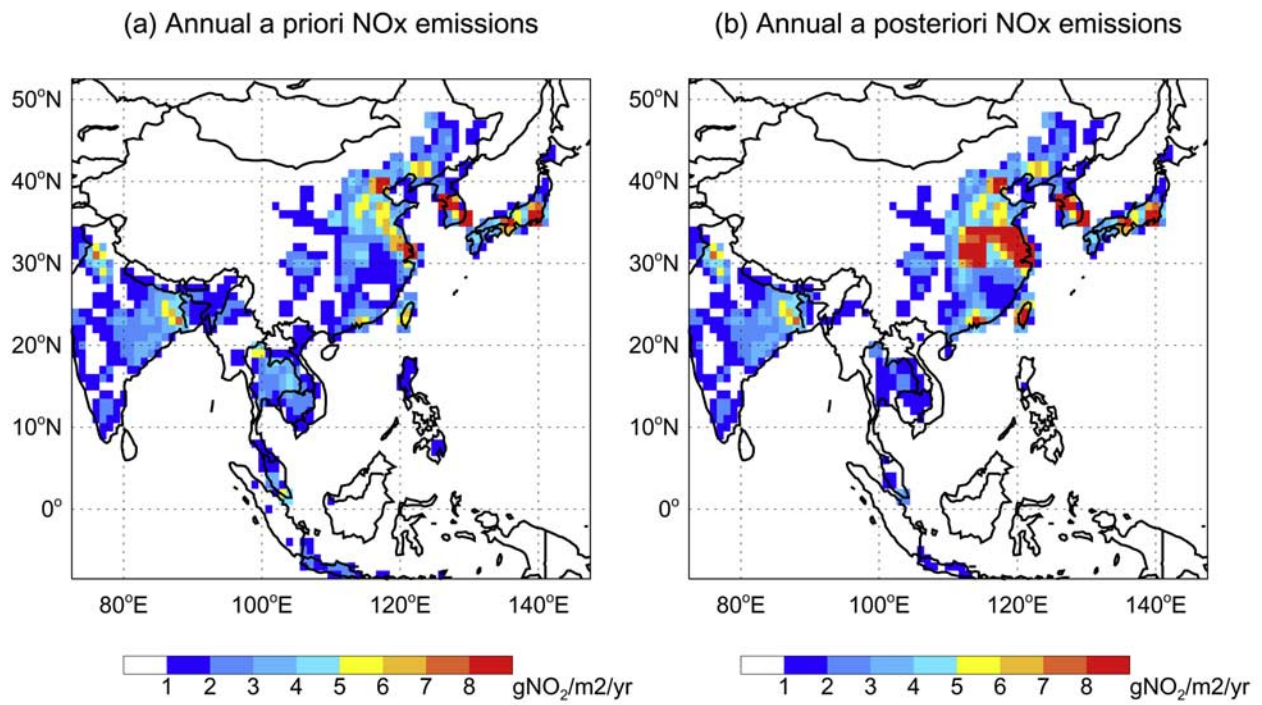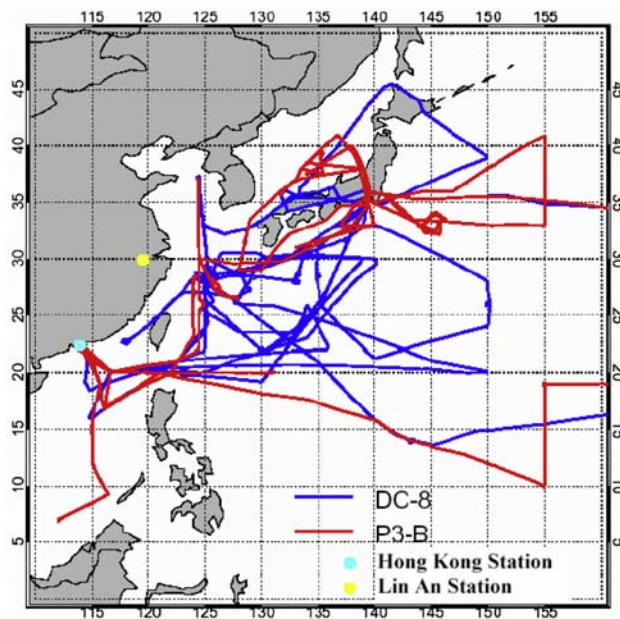
Figure 2. Same as Figure 1, but for NO$_x$ emissions.

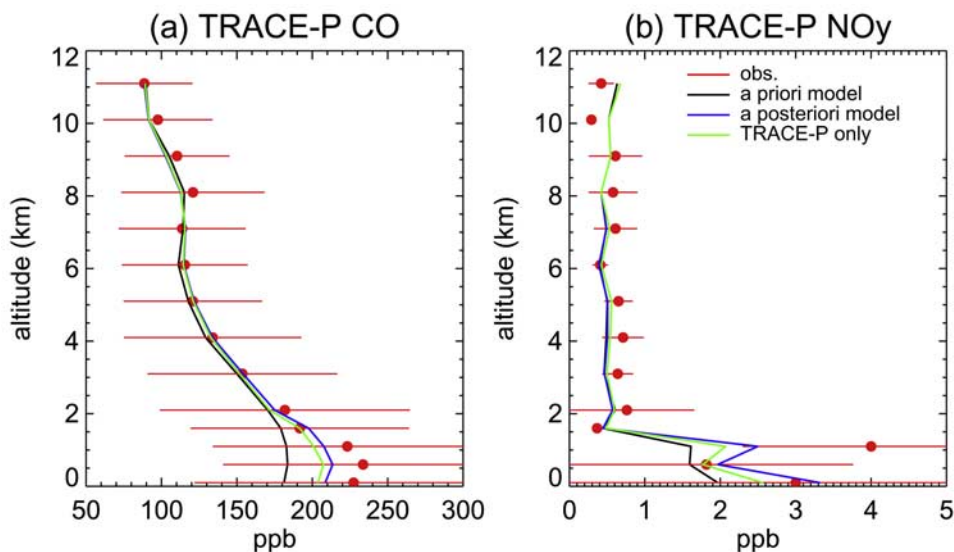**Figure 5.** TRACE-P flight tracks and locations of the two Chinese stations.

Figure 6. Comparison between model simulations and TRACE-P observations of (a) CO and (b) NO$_y$. The data are shown as a function of altitude. Red circles are mean concentrations of observations, and red horizontal lines indicate 1-σ values around the mean. Black lines are mean values of simulated concentrations using a priori emissions. Blue lines are mean model results using a posteriori emissions from the inverse analysis in which both TRACE-P and the surface observations are employed. Green lines are mean model results using a posteriori emissions for the "TRACE-P only" case.
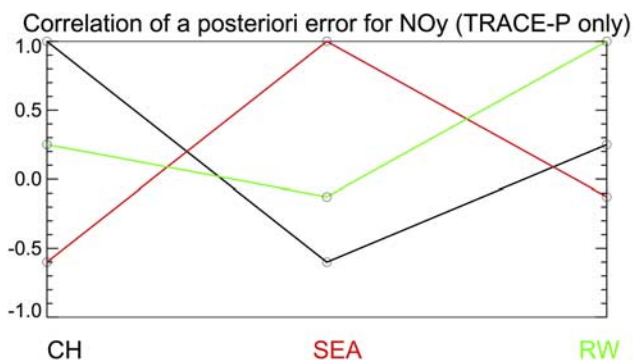

Figure 7. Comparison between simulated and observed (left) NO$_x$/NO$_y$, (middle) HNO$_3$/NO$_y$, and (right) PAN/NO$_y$ ratios made by DC-8 aircrafts in the TRACE-P mission. The data are shown as a function of altitude. Red circles are mean concentrations of observations, and red horizontal lines indicate 1-σ values around the mean. Black lines are mean model results using a priori emissions. Concentrations of HNO$_3$ shown in the middle panel are composite concentrations of gas-phase and aerosol-phase nitrates.

Figure 8. Daily average mixing ratios of observed and modeled CO concentrations at (top) Lin An and (bottom) Hong Kong during 19 February to 30 April 2001. Red lines show observations. Black lines are simulated concentrations using a priori emissions. Blue lines are model results using a posteriori emissions from the inverse analysis in which both TRACE-P and the surface observations are employed. Green lines are mean model results using a posteriori emissions for the ''TRACE-P only'' case.

Figure 9. Daily average mixing ratios of observed and modeled NO$_y$ concentrations at (top) Lin An and (bottom) Hong Kong during 19 February to 30 April 2001. Red lines show observations. Black lines are simulated concentrations using a priori emissions. Blue lines are model results using a posteriori emissions from the inverse analysis in which both TRACE-P and the surface observations are employed. Green lines are model results using a posteriori emissions for the "TRACE-P only" case.

Figure 11. Individual rows of the correlation matrix for the inversion of NO$_y$ sources using only the TRACE-P aircraft data. Different colors distinguish rows of the matrix, with the corresponding columns indicated on the x axis. Lines connect the symbols for clarity and do not have any physical significance.

Figure 12. (top) Individual rows of the averaging kernel matrix **A** for the inversion of CO sources and (bottom) individual rows of the error correlation matrix. Different colors distinguish rows of the matrix, with the corresponding columns indicated on the x axis. Lines connect the symbols for clarity and do not have any physical significance. The five-element state vector for CO includes total sources from Southeast Asia (SEA), north China (N. CH), central China (CN. CH), south China (S. CH), and the rest of the world (RW).

Figure 13. Same as Figure 12, but for the state vector of NO$_y$ inversion. The four-element state vector for NO$_y$ includes total sources from central China (CN. CH), south China (S. CH), Southeast Asia (SEA), and the rest of the world (RW).
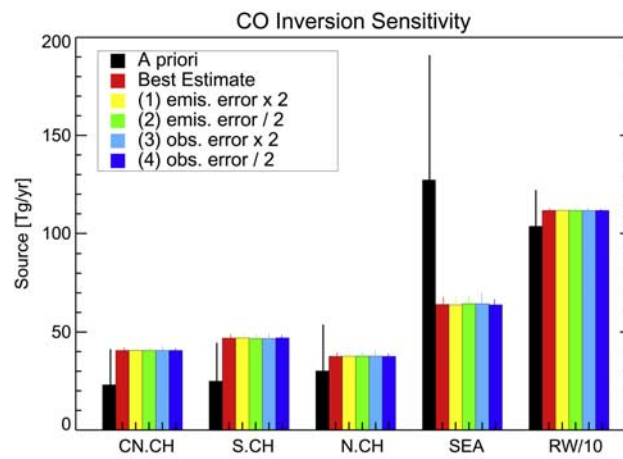
Figure 14. Sensitivity of the calculated a posteriori sources of CO to the error estimates in the inverse model. Vertical bars denote 1-σ value from $\hat{S}$. The range of solutions is summarized in Table 1. Elements in the abscissa are as in Figure 1.
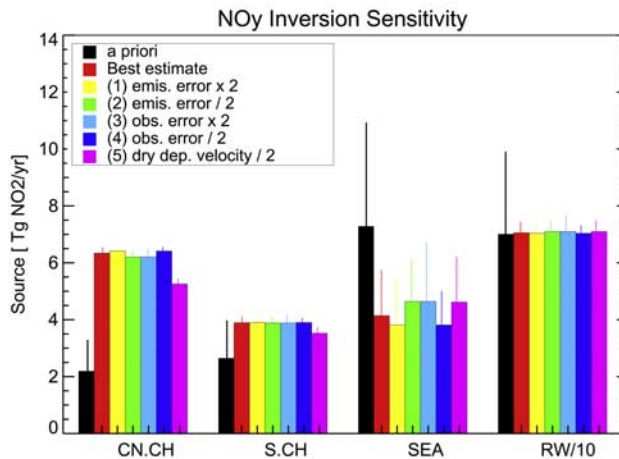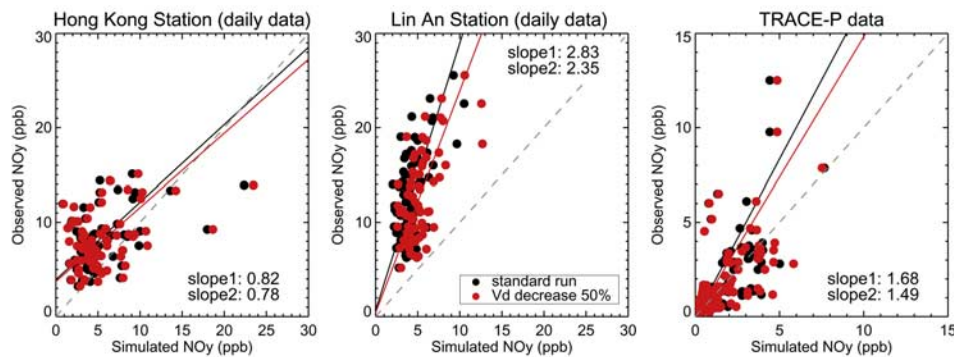
Figure 15. Sensitivity of the calculated a posteriori sources of NO$_y$ to the error estimates in the inverse model. Vertical bars denote 1-σ value from $\hat{S}$. The range of solutions is summarized in Table 2. Elements in the abscissa are as in Figure 1.

Figure 16. Scatterplots of observed NO$_y$ concentrations versus model results obtained from the standard simulation (black circles) and observed NO$_y$ concentrations versus model results using 50% decreased deposition velocity (V_d) for NO$_y$ species (red circles). Data are separately presented with the Hong Kong station in the left panel, Lin An station in the middle panel, and the TRACE-P mission in the right panel. The slopes between observation and model are also shown: "Slope1" denotes the slope between observation and standard model simulation, and "slope2" denotes that between observation and model simulation with decreased V_d.
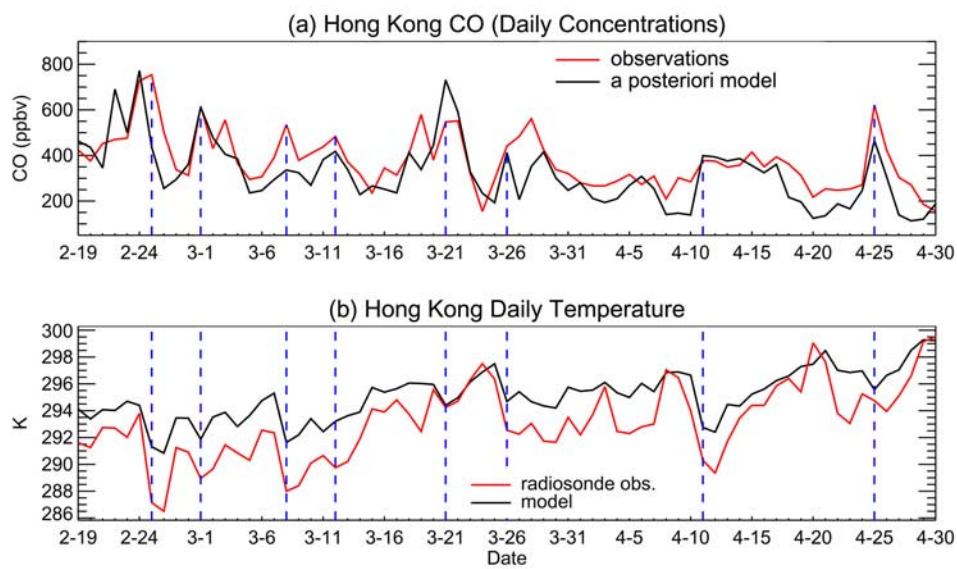
Figure 18. (a) Daily CO concentrations and (b) daily average surface temperatures at Hong Kong. Observations are shown in red, and model predictions are shown in black. The ''cold events'' are indicated by blue dashed lines.
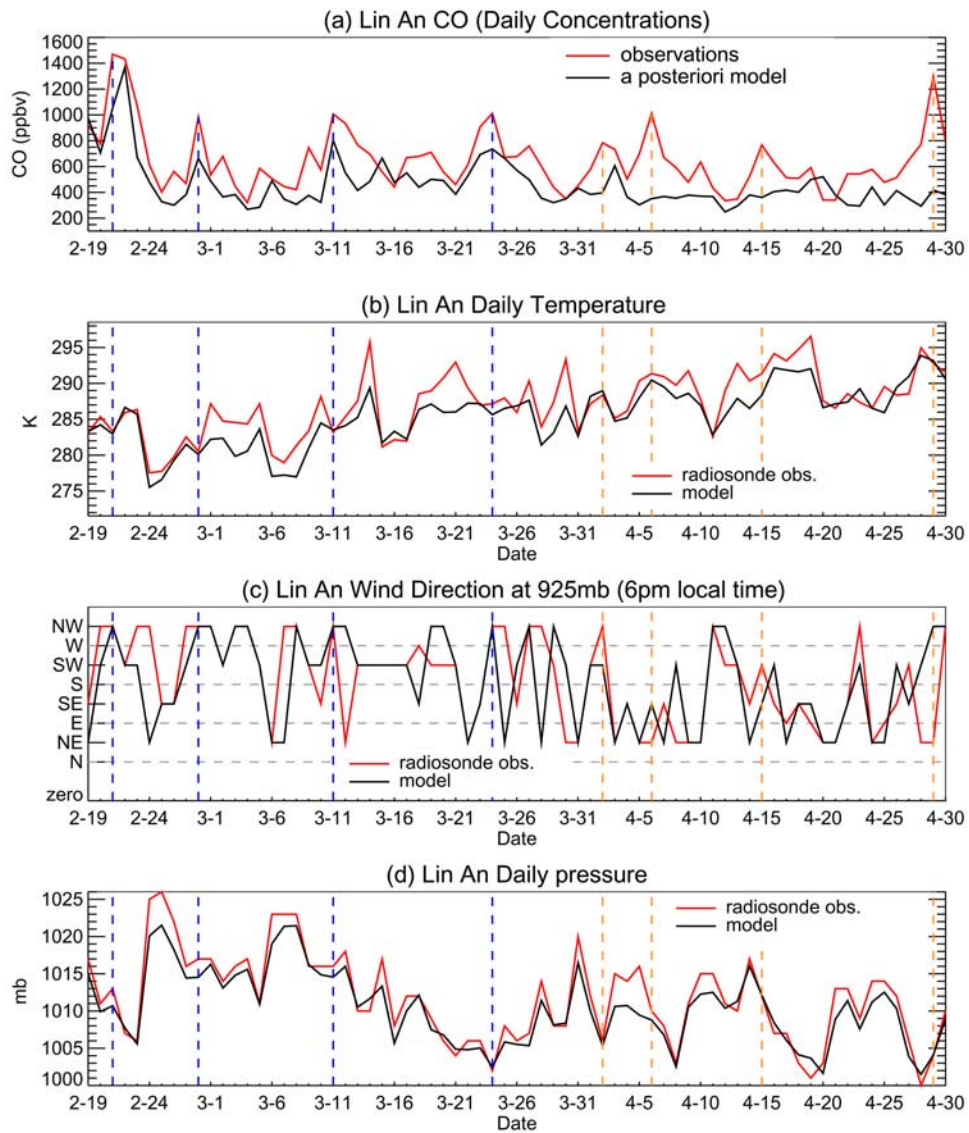
Figure 19. (a) Daily CO concentrations, (b) daily average surface temperatures, (c) wind directions at 925 mbar, and (d) surface pressure at Lin An. Observations are shown in red, and model predictions are shown in black. The "cold events" are indicated by blue dashed lines, and "warm events" are indicated by orange dashed lines.
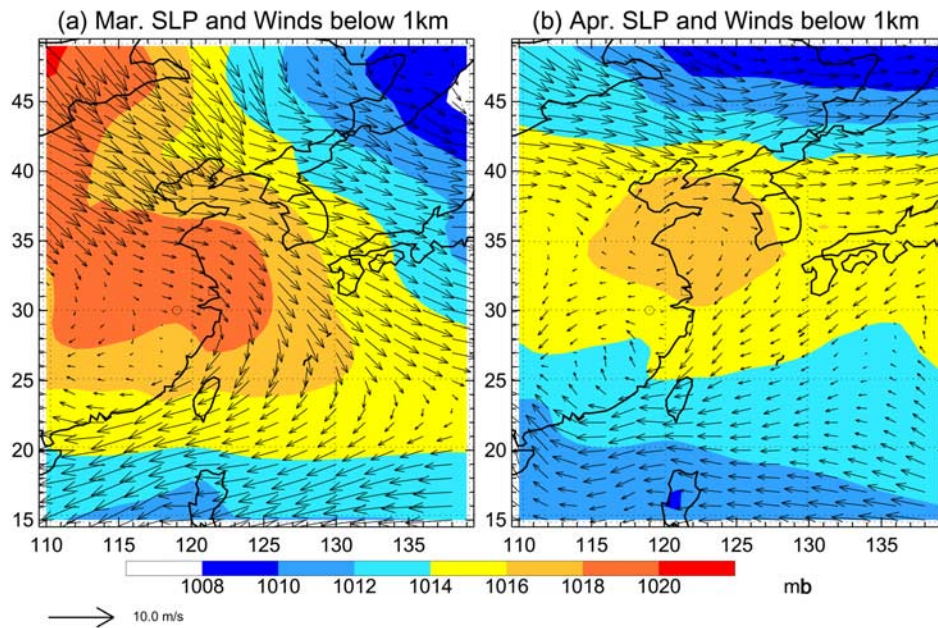
Figure 20. Sea level pressure (SLP; color coding) and wind patterns below 1 km (black arrows) for (a) March and (b) April 2001. The data shown are from the GEOS-3 assimilated meteorology. The locations of Lin An (119°E, 30°N) and Shanghai (121.5°E, 31.4°N) are indicated by an open circle and an open square, respectively.
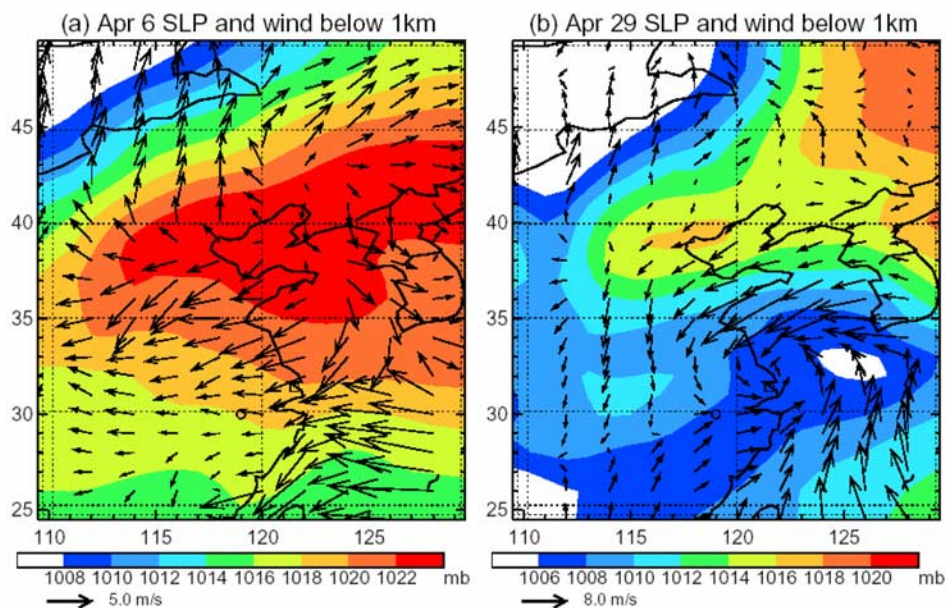

Figure 21. Sea level pressure (color coding) and wind patterns below 1 km (black arrows) for (a) 6 April and (b) 29 April 2001. The data shown are from the GEOS-3 assimilated meteorology. The locations of Lin An (119°E, 30°N) and Shanghai (121.5°E, 31.4°N) are indicated by an open circle and an open square, respectively. Note that the two figures have a different color scale for SLP and arrow length for wind speed.